nature chemical biology

Article

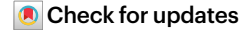
https://doi.org/10.1038/s41589-023-01346-x

Plasmodesmata mediate cell-to-cell transport of brassinosteroid hormones

Received: 11 July 2022

Accepted: 21 April 2023

Published online: 26 June 2023



Yaowei Wang^{1,2}, Jessica Perez-Sancho ® ³, Matthieu Pierre Platre ® ⁴, Brenda Callebaut⁵, Marija Smokvarska³, Karoll Ferrer ® ⁶, Yongming Luo^{1,2,7}, Trevor M. Nolan ® ³, Takeo Sato⁻, Wolfgang Busch ® ⁴, Philip N. Benfey ® ³, Miroslav Kvasnica ⁶, Johan M. Winne ⁶, Emmanuelle M. Bayer ® ³, Nemanja Vukašinović ® ¹,2 ☒ & Eugenia Russinova ® ¹,2 ☒

Brassinosteroids (BRs) are steroidal phytohormones that are essential for plant growth, development and adaptation to environmental stresses. BRs act in a dose-dependent manner and do not travel over long distances; hence, BR homeostasis maintenance is critical for their function. Biosynthesis of bioactive BRs relies on the cell-to-cell movement of hormone precursors. However, the mechanism of the short-distance BR transport is unknown, and its contribution to the control of endogenous BR levels remains unexplored. Here we demonstrate that plasmodesmata (PD) mediate the passage of BRs between neighboring cells. Intracellular BR content, in turn, is capable of modulating PD permeability to optimize its own mobility, thereby manipulating BR biosynthesis and signaling. Our work uncovers a thus far unknown mode of steroid transport in eukaryotes and exposes an additional layer of BR homeostasis regulation in plants.

Brassinosteroids (BRs) are steroidal phytohormones that are crucial for plant growth and regulate diverse developmental processes, such as cell elongation, cell division, photomorphogenesis and xylem differentiation, as well as biotic and abiotic stress responses¹. BRs are perceived by the plasma membrane-localized receptor kinase BR INSENSITIVE 1 (BRI1) and its coreceptor BRI1-ASSOCIATED RECEPTOR KINASE 1 (BAK1) in the apoplast, triggering sequential phosphorylation between BRI1 and BAK1 (ref. 1). This step is required for BRI1 activation and leads to downstream phosphorylation and dephosphorylation events that activate the transcription factors, such as BRASSINAZOLE RESISTANT 1 (BZR1) and BRI1-EMS-SUPPRESSOR 1 (BES1)/BZR2, either to induce or to repress genes in the nucleus as the final outcome of the BR response².³.

Normally, the hormone level at any given site within the plant is determined by the relative rates of biosynthesis, catabolism and transport⁴. Until now, a negative transcriptional feedback loop has been considered the main regulatory mechanism of BR biosynthesis and catabolism, in which the transcription of BR biosynthetic and catabolic genes is directly regulated by BES1 and BZR1 (refs. 5,3). Nevertheless, in the *Arabidopsis thaliana* root, the elongation zone is the site of maximum BR biosynthetic expression⁶ and signaling levels, indicating that additional mechanisms control the expression of biosynthetic enzymes. In the root meristem, the expression domains of BR biosynthetic enzymes are separated, implying cell-to-cell movement of hormone precursors⁶ to allow the biosynthetic pathway completion. Hence, the question arises if BR homeostasis in the root meristem is

¹Department of Plant Biotechnology and Bioinformatics, Ghent University, Ghent, Belgium. ²Center for Plant Systems Biology, VIB, Ghent, Belgium. ³Laboratoire de Biogenèse Membranaire, Unité Mixte de Recherche 5200, Université de Bordeaux, Centre National de la Recherche Scientifique, Villenave d'Ornon, France. ⁴Plant Molecular and Cellular Biology Laboratory and Integrative Biology Laboratory, Salk Institute for Biological Studies, La Jolla, CA, USA. ⁵Department of Organic and Macromolecular Chemistry, Ghent University, Ghent, Belgium. ⁶Laboratory of Growth Regulators, Institute of Experimental Botany, The Czech Academy of Sciences and Palacký University, Olomouc, Czech Republic. ⁷Faculty of Science, Hokkaido University, Sapporo, Japan. ⁸Department of Biology, Duke University, Durham, NC, USA. ⁹Howard Hughes Medical Institute, Duke University, Durham, NC, USA. ☑e-mail: nemanja.vukasinovic@psb.vib-ugent.be; eurus@psb.vib-ugent.be also mediated by short-distance BR transport, as well as what is the mode of BR movement between neighboring cells.

BRs are derived from campesterol and converted to brassinolide (BL), the most bioactive BR, after a series of reactions, including reduction, hydroxylation, epimerization and oxidation⁷. All enzymes involved in BR biosynthesis, except the steroid $5 - \alpha$ -reductase, de-etiolated 2 (DET2), are members of the cytochrome P450 (CYP) protein superfamily⁷. The CYPs are well conserved and are predominantly localized in the endoplasmic reticulum (ER)⁸ membrane. For two of the BR CYPs, DWARF4 (DWF4) and CYP85A2, an ER localization has already been demonstrated^{9,10}. Nonetheless, how BRs exit the cell after their synthesis in the ER membranes and how they are transported between neighboring cells is still unknown. The mammalian steroid hormones, after their release from steroidogenic cells, are transported to the target cells through the blood by their carrier proteins ¹¹. However, no homologs of the mammalian steroid carrier proteins are found in plants, and BRs do not undergo long-distance movements¹².

Multicellular organisms rely on cell-to-cell communication to coordinate growth and development across tissues and organs¹³. In plants, plasmodesmata (PD) are critical cytoplasmic communication channels¹⁴. PD cross the cell walls of adjacent cells and enable intercellular movement of nutrients, hormones, RNAs, proteins, metabolites and viruses¹⁵⁻¹⁹. The typical structure of PD consists of a cytoplasmic sleeve, a plasma membrane leaflet and a desmotubule, a membranous cortical ER-derived rod, connecting adjacent cells²⁰. PD connectivity is exceptionally dynamic, responds to both internal and external stimuli and is regulated by the deposition of callose, a β -(1,3)-glucan polymer, in the PD neck²⁰. Localized production of the polymer by callose synthases can narrow the cytoplasmic sleeve, whereas degradation mediated by β-1,3-glucanases can widen the channel²⁰. Nevertheless, PD conductivity is not directly correlated with the size of the cytoplasmic sleeve²¹, and how exactly PD mediate the exchange of molecules between neighboring cells remains poorly understood. PD number is also controlled because, for instance, secondary PD are often formed during cell growth either to maintain or to increase the PD density in expanding cell walls²². Whether BR precursors are transported via PD to complete the biosynthetic pathway or initiate signaling in adjacent cell files is not known.

Here we corroborate the subcellular localization of BR biosynthetic enzymes in the ER membranes, where hormone biosynthesis likely occurs. By combining genetic and bioorthogonal chemistry approaches, we demonstrate that PD are involved in the short-distance transport of BR precursors, which is required for biosynthetic pathway completion. Finally, we provide evidence that the intracellular BR content negatively regulates PD permeability, possibly through BR signaling inducing callose deposition in the cell walls near the neck zone of the PD and, ultimately, affecting its own mobility and biosynthesis efficiency. Our work reveals an unidentified transport mode of steroidal hormones in eukaryotes and presents an additional layer of BR biosynthesis regulation in plants.

Fig. 1|**PD permeability modulates BR signaling. a**, Increased callose biosynthesis at plasmodesmata in *isals3m* expressing plants inhibits the exchange of molecules between neighboring cells (left). Aniline blue staining of callose deposition in endodermis of the root tips of *pEN7:icals3m* plants upon EST ($5 \mu M$) or DMSO (mock) treatment for 48 h (right). Scale bars, $100 \mu m$. **b**, Induction of callose deposition ($48 \cdot h$ EST treatment) in the endodermis of *pEN7:icals3m* seedlings causes root growth defects. Root tips were marked immediately after the transfer (white bars). Scale bar, 1 cm. c.d, Quantification of the primary root length (c) and mature cortical cell length (d) of seedlings shown in c0. All individual data points are plotted. Horizontal and error bars represent the means and s.d., respectively. c1, number of roots used in c2 and cells used in c3. The significant differences were determined with one-way analysis of variance (ANOVA) and Tukey's multiple comparison tests. c2, Phosphorylation status of BES1 detected by immunoblotting with c3-BES1 antibody. Tubulin detected with c4-tubulin antibody was used as a loading control. Root tips of 5-d-old *Arabidopsis*

Results

Symplastic communication modulates BR signaling

To determine the subcellular localization of BR biosynthetic enzymes, we co-expressed the GFP-tagged rotundifolia 3 (*ROT3*) and DWF4 with the mCherry-tagged ER membrane-resident marker cinnamate 4-hydroxylase (C4H)²³ in *Nicotiana benthamiana* (tobacco) leaves (Extended Data Fig. 1a,c) and in roots of transgenic *Arabidopsis* plants (Extended Data Fig. 1b,d). As reported earlier for some *Arabidopsis* CYP proteins 9.10.24, both enzymes localized in the ER membrane, marking it as the likely site of BR biosynthesis within cells.

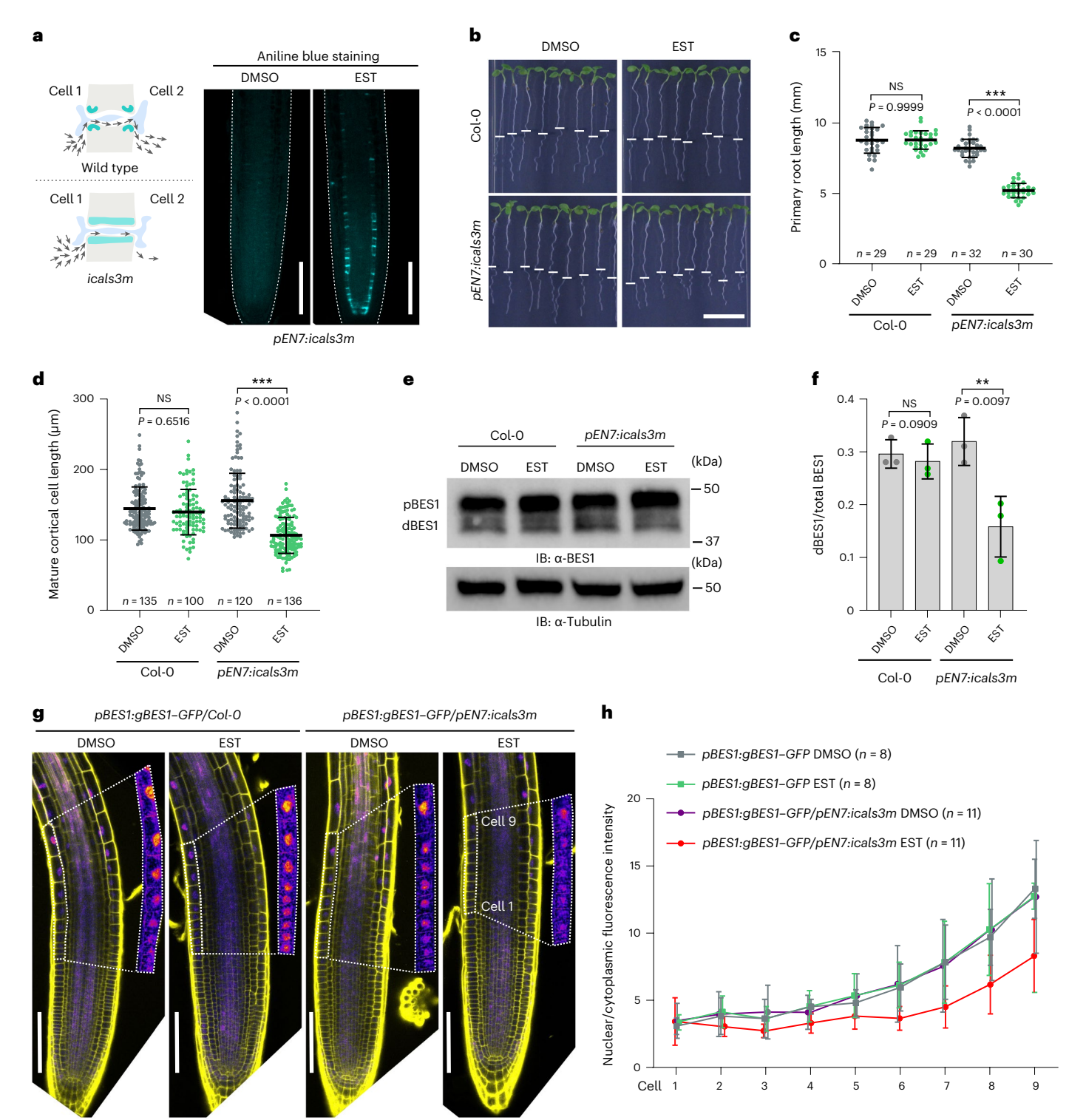
Previously we showed that BRs move between neighboring cell files in the roots of *Arabidopsis*⁶. Given that BR biosynthetic enzymes are localized in the ER membranes and the hormone is synthesized intracellularly, we hypothesized that the exchange of BRs between adjacent cell files occurs via PD. First, we asked whether the sites of BR biosynthesis might coincide with PD, which could facilitate hormone transport. To this end, we examined the colocalization of the BR biosynthetic enzyme, DWF4-GFP, and the mCherry-tagged PD marker, PD-located protein 1 (PDLP1)14, in tobacco leaves (Extended Data Fig. 1e) and estimated the PD enrichment by calculating the PD index²⁵ (Extended Data Fig. 1f). DWF4-GFP exhibited a higher PD index than the ER lumen marker HDEL-BFP, indicating a PD association, but these values were lower than those for MCTP3-GFP, a PD-resident protein²⁶. However, in the roots of *Arabidopsis* plants co-expressing ROT3-GFP and DWF4-GFP with PDLP1-mCherry, no clear enrichment of the GFP signal at the PD was found (Extended Data Fig. 1g,h). These findings suggest that the BR biosynthetic machinery might be loosely associated with PD and only in certain cell types. Second, to test if BRs move through the PD, we examined the root growth of transgenic Arabidopsis plants expressing the gain-of-function callose synthase 3 (CALS3) from the estradiol (EST)-inducible endodermis 7 (EN7) promoter (pEN7:icals3m) that can block PD by callose deposition in the PD neck in the endodermis after induction²⁷ (Fig. 1a). The phenotypic analysis showed that after a 48-h EST treatment, primary root growth was arrested and that the length of the mature cortical cells was substantially shorter than that of the mock-treated plants (Fig. 1b-d). To investigate whether blocking PD in the endodermis affects BR signaling, we analyzed BR-specific phenotypes in the root meristems⁶. To look at relatively early BR signaling responses and minimize the pleiotropic effect of PD closure, we decreased the induction time to 12 h, as this condition was sufficient to observe callose production (Extended Data Fig. 2c). Callose deposition reduced the average length of meristematic cortical cells and slightly increased the root diameter (Extended Data Fig. 2a,b), suggesting decreased BR signaling levels in pEN7:icals3m roots after induction. We then analyzed the accumulation of dephosphorylated BES1 (dBES1), which can be used as a readout for BR signaling activation². Compared to the wild-type accession Columbia-0 (Col-0), BES1 was slightly less dephosphorylated in the

seedlings grown as in **a** and induced for 12 h were used. **f**, Quantification of BES1 dephosphorylation in **e** presented as a ratio of dBES1 relative to the total BES1. The significant difference was determined with a two-tailed Student's paired t-test analysis. Error bars represent s.d. **g**, Confocal images of root tips of pBES1:gBES1-GFP/Col-0 and pBES1:gBES1-GFP/pEN7:icals3m seedlings. Five-day-old seedlings were transferred to agar media containing EST (5 μ M) or DMSO (mock) and imaged after 12 h. Cell walls were stained with Pl. Nine cells used for fluorescence intensity measurements in **h** are shown in inset panels (1.5× enlarged). In the inset panels, only GFP signal is shown. Brightness and contrast were equally adjusted for each treatment. Scale bars, 100 μ m. **h**, Quantification of nuclear/cytoplasmic BES1–GFP fluorescence intensity ratio of epidermal cells in the root transition zone (nine cells shown in the inset panels in **g**). Values and error bars represent means and s.d., respectively. n, number of roots used for each treatment. ***P< 0.001 and **P< 0.01 for **c**,**d** and **f**. For **b**-h, experiments were performed in three repeats with similar results. IB, immunoblotting.

callose-induced roots (Fig. 1e,f), indicating a decrease in BR signaling. In addition, we introduced the *pBES1:gBES1-GFP* reporter²⁸ into the *pEN7:icals3m* plants²⁷ and examined the nuclear accumulation of BES1, which is also used as an indicator of BR signaling activation². The nuclear/cytoplasm fluorescent intensity ratio of BES1-GFP was reduced in root epidermal cells after 12 h of EST treatment (Fig. 1g,h), possibly as a result of decreased BR signaling. These findings suggest that the reduced PD permeability might compromise BR signaling, probably due to impaired transport of BRs through the PD.

Limiting the PD transport can be detrimental to root growth because numerous signaling components and nutrients are transported through these intercellular channels 15-19. To overcome, or at least

limit the pleiotropic effects of callose-plugged PD on root growth and uncouple BR-specific effects, we ectopically expressed the PD-located protein 5 (PDLP5)–BFP²⁹ fusion to induce overaccumulation of callose at the PD in the native domain of the BR biosynthetic enzyme, constitutive photomorphogenesis and dwarfism (CPD) in the *pCPD:CPD-GFP/cpd* (Extended Data Fig. 2d,e). This fusion allowed us to spatially link CPD enzyme activity with ectopic callose deposition in the central part of the root, the stele, and minimize the interruption of movement of other PD-transported molecules. Roots of this transgenic line grew more slowly than those of *pCPD:CPD-GFP/cpd* (Extended Data Fig. 2f,g) and exhibited BR-deficient phenotypes (Extended Data Fig. 2h,i). Additionally, an increase in phosphorylated BES1 (pBES1)



indicated reduced BR signaling levels in roots expressing PDLP5-BFP (Extended Data Fig. 2j).

To validate our findings that impaired symplastic transport negatively regulates BR signaling, we compared the effect of PDLP5–BFP expression under the *CPD* promoter in *pCPD:CPD-GFP/cpd* and *pSCR:CPD-mCherry/cpd* backgrounds. When the CPD-mCherry⁶ enzyme was ectopically expressed in the endodermis, milder growth defects were observed (Extended Data Fig. 2d-i), as well as less affected BR signaling levels (Extended Data Fig. 2j). CPD is a BR biosynthetic enzyme with the most restricted expression domain in the stele, whereas all other enzymes are, at least partially, expressed in other tissues⁶. Therefore, displacement of CPD enzyme expression to the endodermis allowed possible movement of BR precursors and completion of the pathway by bypassing PDLP5–BFP-induced callose deposition and the reduced PD connectivity in the stele, respectively.

Subsequently, we assessed the BR-related phenotypes and BR signaling in transgenic Arabidopsis plants overexpressing the callose-degrading enzyme plasmodesmal-localized β-1,3-glucanase 1 (PdBG1)³⁰ (p35S:PdBG1-mCitrine/Col-0, PdBG1-OE), which have increased PD permeability as a result of enhanced callose turnover (Extended Data Fig. 3a,b). The phenotypic analysis revealed that the length of the primary roots of PdBG1-OE seedlings was substantially longer than that of the wild type, with longer meristematic cells and a slightly smaller root radius (Extended Data Fig. 3d-f), thus, resembling, to a certain extent, the phenotype of plants with constitutive BR responses⁶. In agreement, the PdBG1–OE plants accumulated more dBES1 than the control (Extended Data Fig. 3g,h), whereas the expression of DWF4 was downregulated (Extended Data Fig. 3i), indicating that the increased cell-to-cell connectivity positively affected BR signaling. Taken together, our results show that PD permeability can moderately modulate BR signaling levels.

PD mediate BR movement

We hypothesized that the impaired BR signaling in different PD mutants was due to the altered mobility of BR precursors. To test this assumption, we employed BR precursor feeding experiments with 22-hydroxycampesterol[22-OHCR(compound1);SupplementaryNote1], which is the product and the substrate of DWF4 and CPD enzymes, respectively (Extended Data Fig. 4a). As expected, exogenous 22-OHCR (500 nM) was able to rescue the root growth of dwf4 and to dephosphorylate BES1 in this mutant, similarly to BL (500 pM), whereas it was inactive when applied to the *cpd* mutant (Extended Data Fig. 4b-d). Next, the inducible pEN7:icals3m construct was introduced into the dwf4 mutant to conditionally perturb PD permeability in the endodermis. We postulated that after induction of callose deposition at PD in the endodermis, exogenous BL would reach epidermal and cortical cell layers, where BR signaling is sufficient to rescue the root growth of BR-related mutants³¹ (Fig. 2a). Conversely, the inactive BR precursor 22-OHCR would need to move to the stele, where the CPD enzyme is expressed, to be converted into the following BR precursor and, finally, to BL to rescue dwf4 root growth. In a scenario in which BRs move via the PD, callose-induced PD blockage in the endodermis would interrupt the biosynthetic pathway and exogenous 22-OHCR would not rescue the dwf4 defects (Fig. 2a). Consistent with this hypothesis, we found that without callose induction, both exogenous 22-OHCR (500 nM) and BL (500 pM) rescued the root growth defects of pEN7:icals3m/dwf4 plants, including primary root and mature cortical cell lengths (Fig. 2b-d). However, after blocking PD in the endodermis, 22-OHCR was less effective in rescuing the dwf4 root growth defects than BL (Fig. 2b-d and Extended Data Fig. 4e-g).

To further corroborate the different capacities of exogenous BL and 22-OHCR to rescue *dwf4* when PD were closed in the endodermis, we evaluated BR signaling by immunoblot analysis of the phosphorylation status of BES1. Because the *EN7* promoter is only active in the root tip, we collected root tips for immunoblotting. In accordance

with the observed root phenotypes, BR signaling was less efficiently recovered by 22-OHCR than by BL after callose induction (Fig. 2e). Then, we introduced the *pBES1:gBES1-GFP* construct into *pEN7:icals3m/dwf4* plants and quantified the nuclear accumulation of BES1-GFP in the root epidermis as a BR signaling readout. As predicted, BR signaling in the mock-treated *pBES1:gBES1-GFP/pEN7:icals3m/dwf4* seedlings was enhanced by exogenous BL and 22-OHCR with equal efficiency (Fig. 2f,g), but it was only partially complemented by 22-OHCR in the EST-treated seedlings (Fig. 2f,g).

Taken together, these results suggest that PD closure renders BR biosynthesis inefficient, possibly due to the necessity for BR precursors to be exchanged through PD between adjacent root cell files.

Direct visualization of BR movement

To validate the PD-mediated intercellular transport of BRs and directly visualize BRs in Arabidopsis roots, we used a bioorthogonal chemistry approach. To this end, castasterone-alkyne (CSA, 2) was synthesized by the introduction of an alkyne group attached to a linker connected to the C-6 position of the castasterone (CS) molecule (Fig. 3a and Supplementary Note 2), which is the direct precursor of BL (Extended Data Fig. 4a). CSA can be visualized after cycloaddition or a click reaction between its alkyne and the azide group of the commercially available green-emitting fluorescent dye azide-BODIPY-fluorescein (azide-BDP-FL)³² to generate CS-BDP-FL (3; Fig. 3a). Although slightly less potent than CS, CSA retained biological activity, because it rescued the short-root phenotype of the dwf4 mutant and induced BES1 dephosphorylation (Fig. 3b and Extended Data Fig. 5a,b). Subsequently, a click reaction was carried out on transgenic Arabidopsis lines with perturbed PD permeability. Initially, the pEN7:icals3m line was used, which has increased callose deposition (Fig. 1a) and closed PD in the endodermis after EST induction. In the absence of CSA, no signal was detected in the mock- and EST-treated seedlings (Fig. 3c), indicating that the azide-BDP-FL fluorescent dye did not bind nonspecifically, whereas in the presence of CSA and after a click reaction with azide-BDP-FL, the CS-BDP-FL signal occurred only in epidermal and cortical cells in EST-treated roots, but it was ubiquitous in all cell files in noninduced roots (Fig. 3c,d). These findings suggest that closed PD in the endodermis block the CSA movement from the cortex to the inner tissues.

Consequently, a similar click reaction was carried out with a line expressing icals3m from the WEREWOLF (WER) promoter³³, pWER:icals3m. This line specifically accumulated callose in epidermal cells, presumably blocking PD in this tissue (Extended Data Fig. 5c), and caused root growth inhibition (Extended Data Fig. 5d,e). In the root tips of the pWER:icals3m seedlings treated with CSA followed by a click reaction, the fluorescent CS-BDP-FL signal accumulated preferentially in epidermal cells when compared to the Col-0 control (Fig. 3e,f), implying that PD closure in the epidermal cells is sufficient to block CSA from moving to the inner tissues. Notably, the uptake of CSA in the epidermal cells was not compromised by extensive callose deposition (Extended Data Fig. 5f), hinting that the lack of fluorescent signal in the inner tissues of the *pWER:icals3m* line is due to the compromised symplastic transport and not to impaired compound uptake. Finally, CSA click chemistry experiments were conducted with the PdBG1-OE plants³⁰, which have open PD. The accumulation of the fluorescent signal in all cell layers was higher than that of the Col-O control (Fig. 3g,h), suggesting an enhanced accumulation of CSA in the root when the PD aperture is increased. In conclusion, bioorthogonal chemistry allowed the direct visualization of a bioactive BR precursor in plant tissues, confirming the involvement of PD in intercellular BR transport.

BRs modulate PD permeability

As BRs are transported through the PD, we queried whether BRs could, in turn, modulate PD permeability. To investigate this hypothesis, we visualized callose deposition by means of a callose-specific antibody in wild-type Col-0 plants treated with either BL (200 nM) or the

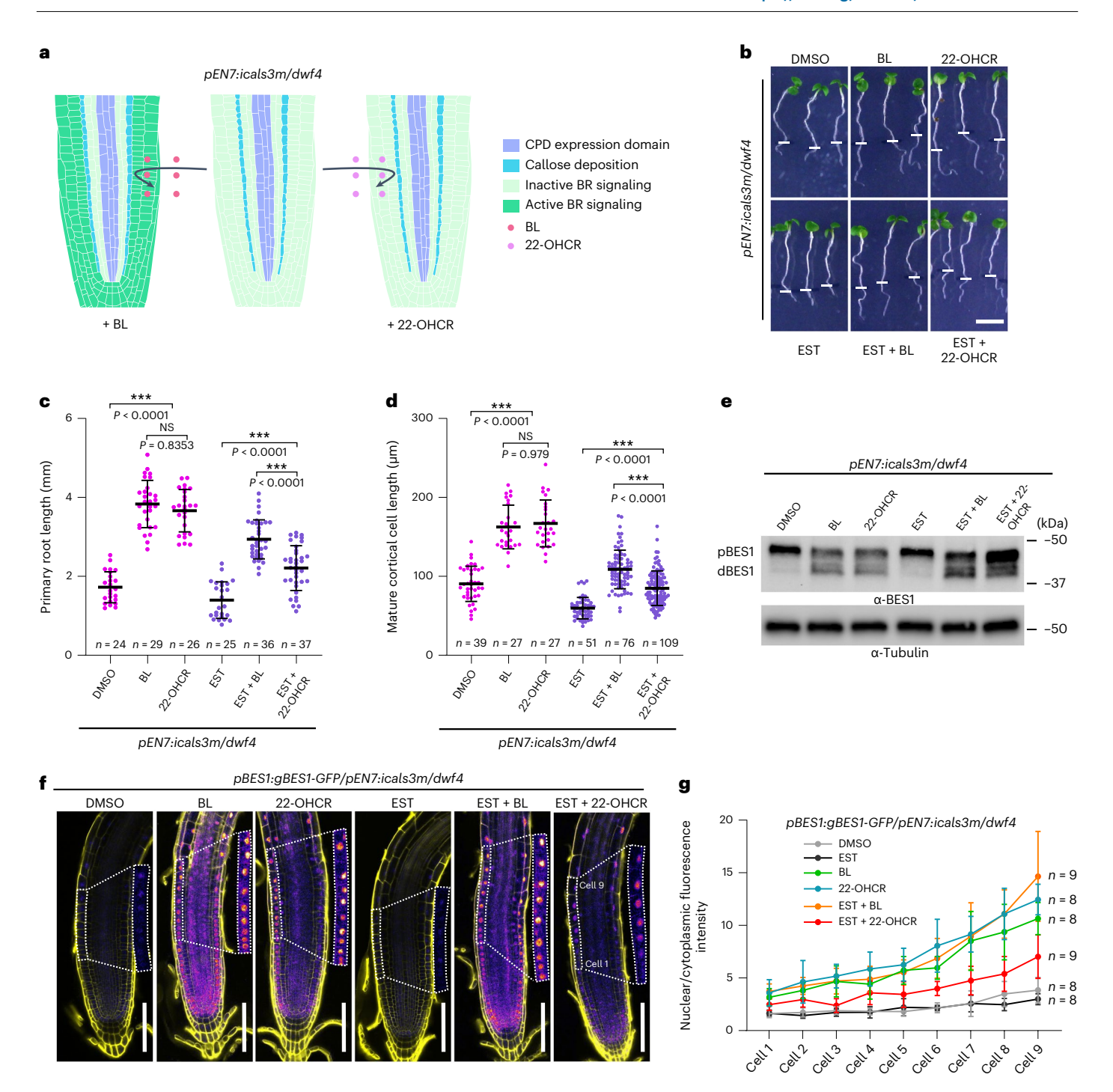
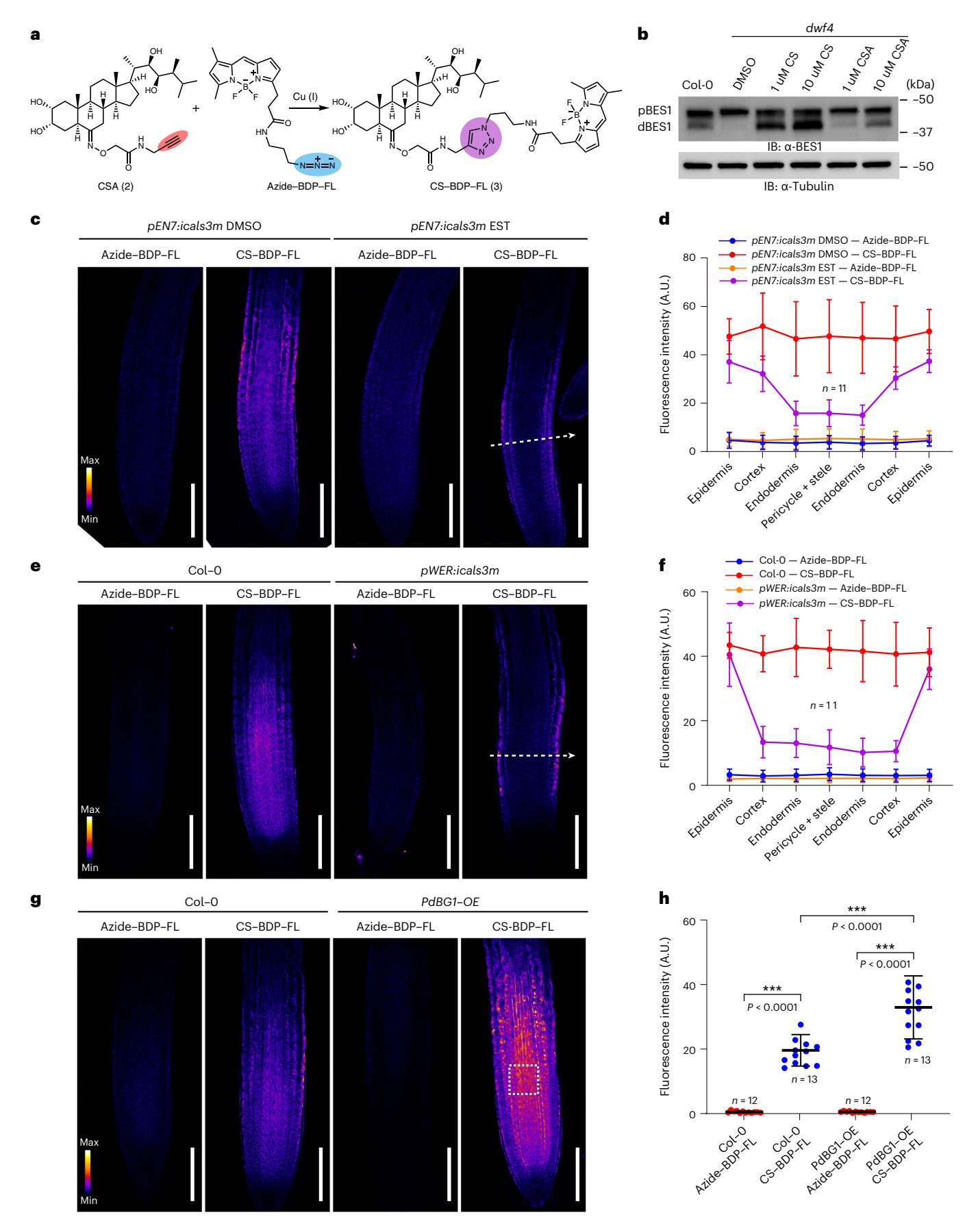


Fig. 2 | **BL** but not its precursor 22-OHCR rescues *dwf4* mutants after PD **closure. a**, Schematic representation of different complementation principles by BL and 22-OHCR of the *dwf4* root upon callose deposition in the endodermis. **b**, The root growth phenotype of *pEN7:icals3m/dwf4* plants in response to exogenous BL and 22-OHCR upon callose induction. Four-day-old seedlings were transferred to an agar medium containing either DMSO (mock) or EST (5 μM) for 24 h. Next, seedlings grown on DMSO were transferred to an agar medium containing DMSO, BL (500 pM) or 22-OHCR (500 nM; upper panel). Seedlings grown on EST were transferred to an agar medium containing EST (5 μM), EST (5 μM) + BL (500 pM) and EST (5 μM) + 22-OHCR (500 nM; lower panel) and grown for 24 h. Root tips were marked immediately after the transfer (white bars). Scale bar, 5 mm. **c**,**d**, Quantification of the primary root (**c**) and the mature cortical cell (**d**) lengths from **b**. Horizontal and error bars represent the means and s.d., respectively. *n*, number of roots used in **c** and cells used in **d**. The

significant differences between the transgenic lines and the wild-type (Col-0) control were determined with ANOVA and Tukey's multiple comparison tests.
****P < 0.001. **e**, Phosphorylation status of BES1 detected by immunoblotting with α -BES1 antibody in root tips. Tubulin detected with α -tubulin antibody was used
as a loading control. **f**, Confocal images of 6-d-old root tips of pBES1:gBES1-GFP/pEN7:icals3m/dwf4 Arabidopsis seedlings treated as in **b**. Cell walls were stained
with Pl. Nine cells used for fluorescence intensity measurements in **g** are shown in
insets (1.5× enlarged). In the inset panels, only the GFP signal is shown. Brightness
and contrast were equally adjusted for each treatment. Scale bars, 100 µm. **g**, Quantification of nuclear/cytoplasmic BES1–GFP fluorescence intensity ratio
of epidermal cells in the root transition zone (nine cells from the inset panels in **f**).
Error bars represent s.d. n, number of roots used for each treatment. For **b-d** and **e-g**, experiments were performed in three and two repeats, respectively, with
similar results.



BR biosynthesis inhibitor BRZ (1 μ M) for 24 h. The immunostaining revealed that BL-treated seedlings exhibited increased callose deposition, whereas the callose levels were substantially reduced after

BRZ treatment (Fig. 4a,b and Extended Data Fig. 6). Consistently, the BR-deficient *dwf4* and *cpd* mutants had almost no callose deposition in their root meristems, but the observed callose deficiency was rescued

Fig. 3 | **Localization of CSA in** *Arabidopsis* **root tips. a**, Chemical compounds used in the bioorthogonal reaction. **b**, CSA is retaining the biological properties of CS. Phosphorylation status of BES1 detected with immunoblotting and α-BES1 antibody. Tubulin detected with the α-tubulin antibody was used as a loading control. Five-day-old wild-type *Arabidopsis* and *dwf4* mutant seedlings were transferred to an agar medium containing CS or CSA at the indicated concentrations and DMSO (mock) for 24 h. **c**, Blocking PD in the endodermis arrests CS-BDP-FL signal in epidermal and cortical cells. Five-day-old seedlings were transferred to an agar medium containing either EST (5 μM) or DMSO (mock) for 24 h. Next, seedlings from each treatment were divided into two and transferred to liquid media containing either CSA (20 μM) or DMSO (mock) for 4 h, followed by a bioorthogonal reaction. **d**, Fluorescence intensity quantification along the white dashed arrow in **c**, positioned at 200 μm away

from the root tip shown in \mathbf{c} . \mathbf{e} , Blocking the PD in epidermal cells arrests CS-BDP-FL signal accumulation in the epidermis. Six-day-old seedlings were incubated in a liquid medium with either CSA (20 μ M) or DMSO (mock) for 4 h followed by a bioorthogonal reaction. \mathbf{f} , Quantification of fluorescence intensity in \mathbf{e} , positioned at 200 μ m away from the root tip shown in \mathbf{e} . \mathbf{g} , Highly permeable PD increase the CSA uptake. Six-day-old PdBG1-OE plants were treated as in \mathbf{e} . \mathbf{h} , Quantification of fluorescence intensity in \mathbf{g} , in which a 50 × 50 μ m² area, 200 μ m away from root tip (white dashed box in \mathbf{g}), was used. The significant differences were determined with ANOVA and Tukey's multiple comparison tests. ***P < 0.001. Scale bars, 100 μ m (\mathbf{c} , \mathbf{e} and \mathbf{g}). Horizontal bars in \mathbf{h} represent the means, and error bars in \mathbf{d} , \mathbf{f} and \mathbf{h} represent the s.d. A.U., arbitrary units; n, number of roots. For \mathbf{b} , \mathbf{e} and \mathbf{f} , the experiment was repeated two times; for \mathbf{c} and \mathbf{d} . four times: and for \mathbf{g} and \mathbf{h} . three times with similar results.

by exogenous BL (Fig. 4a,b and Extended Data Fig. 6). These results indicate that BRs can modulate PD permeability and that high and low BR signaling would induce closure and opening of PD, respectively.

To explore whether the symplastic BR transport is regulated by BR signaling, we performed photoactivation of cytosolic DRONPA-s, a reversibly switchable photoactivatable fluorescent protein in single root cells and monitored the spread of the fluorescent signal to the surrounding cells³⁴ (Fig. 4c). We observed substantially faster spread of the signal in mock-treated Col-O plants in comparison to BL-treated ones (Fig. 4d), demonstrating the ability of BRs to decrease PD permeability. To directly observe the distribution of CSA under conditions of perturbed BR signaling, click chemistry was used. As anticipated, exogenous BL substantially reduced the accumulation of CSA in Col-0 roots when compared with the mock control (Fig. 4e,f). Conversely, CSA accumulation in the root meristems of dwf4 seedlings was stronger than in Col-0 roots (Fig. 4g,h). To examine whether the reduced CSA accumulation is a consequence of increased BR signaling levels and not a competition with BL, we tested CSA accumulation after bikinin (BIK) treatment, which can activate BR signaling downstream of the BRI1 receptor³⁵. Similar to BL, BIK application reduced CSA accumulation in the treated plants (Fig. 4e,f). The BR-induced callose turnover and control of PD permeability are likely under transcriptional control because BR signaling positively regulates expression levels of several callose deposition-related genes in the Arabidopsis root³⁶ (Extended Data Fig. 7 and Supplementary Table 1).

In summary, our findings demonstrate the existence of an additional BR signaling regulatory feedback loop that acts at the PD permeability level and ensures optimal BR biosynthesis by modulating BR movement.

Discussion

Polyhydroxylated steroidal molecules are used as signaling molecules in both mammals and plants to control a plethora of developmental processes^{37–39}. Although these molecules share similar structures, they impact gene expression differently. For example, in mammals, steroidal hormones act in an endocrine manner, namely they are synthesized in

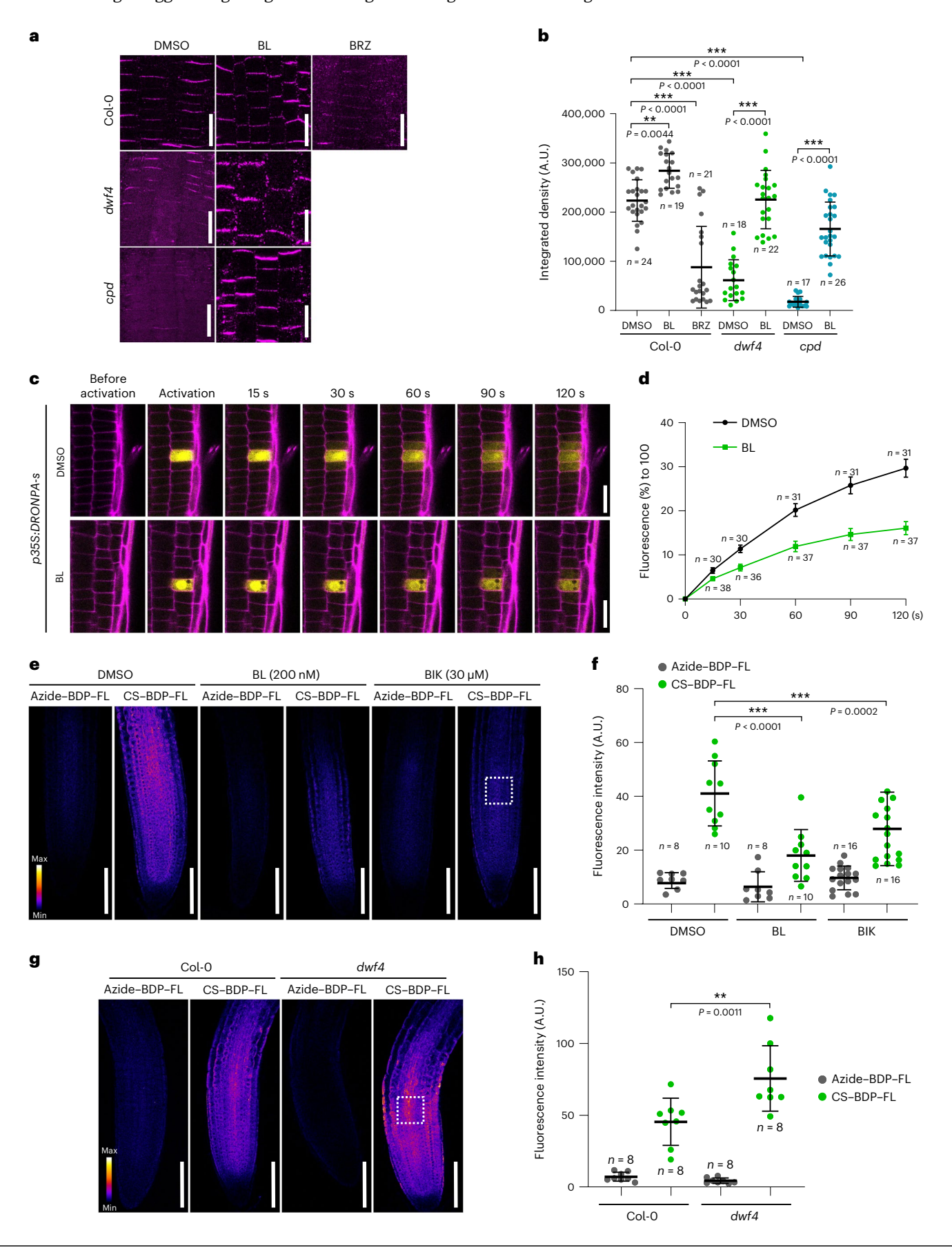
glands, transported by specialized protein carriers and after release into the target cell cytoplasm, they bind to intracellular receptors¹¹. In plants, a family of plasma membrane-localized receptors, including BRI1 and its homologs BRI1-LIKE1 (BRL1) and BRI1-LIKE3 (BRL3), perceive locally produced BRs in the apoplast 40 because plant steroidal hormones do not undergo long-distance transport¹². The textbook knowledge suggests that steroid hormones can freely diffuse across biological membranes due to their hydrophobicity. However, the simple diffusion theory was challenged by finding that the release of the steroid hormone ecdysone in Drosophila melanogaster requires ATP-binding cassette transporter-mediated vesicle loading and calcium-mediated vesicle exocytosis⁴¹, and the cellular uptake of ecdysone needs a membrane solute carrier transporter. In addition, molecular dynamics simulation experiments demonstrated that the flip-flop transitions of steroids, and hence, their ability to diffuse across lipid membranes, are determined by the number of hydroxyl groups in the molecule⁴². Here we confirmed that the BR biosynthetic enzymes are localized in the ER membrane, which is the most likely place for BR biosynthesis. As BR biosynthetic enzymes are expressed in a nonoverlapping fashion along the radial axis of *Arabidopsis* roots, exchange of precursors between cells of different cell files is necessary for the completion of bioactive BR synthesis. Given that BRs are hydrophobic molecules, it is unlikely that they freely move via an apoplastic route between neighboring cells. Alternatively, PD-mediated symplastic transport can ensure the movement of steroid molecules in plants. This pathway enables the cell-to-cell exchange of nutrients, hormones, RNAs, proteins, metabolites and viruses^{15–19}. Therefore, we speculated that the intermediates or bioactive BRs are transported through the PD after synthesis in the PD vicinity. In the scenario of PD-mediated BR transport, perturbation of PD permeability should affect BR signaling. Examination of Arabidopsis plants with altered PD permeability revealed that BR signaling was modulated to a certain extent in plants with perturbed PD permeability, possibly due to the reduced or enhanced ability to transport BRs through the PD. Nevertheless, BR signaling levels were not drastically changed when PD conductivity was altered. The reason for this observation might be the pleiotropic nature of PD mutants and the

Fig. 4 | **BRs regulate PD permeability. a**, Callose immunostaining of *Arabidopsis* wild-type (Col-0), *dwf4* and *cpd* roots using an α-callose antibody. Four-day-old seedlings were transferred to an agar medium containing BL (200 nM), BRZ (1 μM) and DMSO (mock) for 24 h. Scale bars, 20 μm. **b**, Quantification of callose intensity at the PD in **a**. Callose signal at the cell plate was excluded from measurements. **c**, The reversibly switchable photoactivatable fluorescent protein system DRONPA-s movement after activation in a single meristematic cell of the root. Confocal images of 6-d-old root meristems stained with PI are shown. Roots were treated either with mock or BL (200 nM) for 24 h before imaging. Scale bars, 20 μm. **d**, Normalized values of the mean fluorescence intensity of the DRONPA-s are extracted from the adjacent cells next to the activated cell. For each time point, n > 15. Error bars represent the standard error of the mean (s.e.m). **e**, Reduction of the CSA uptake after BL and BIK treatment. Five-day-old seedlings were

transferred to an agar medium containing BL (200 nM), BIK (30 μ M) or DMSO (mock) for 24 h, followed by the bioorthogonal reaction to form CS-BDP-FL. f, Quantification of fluorescence intensity of images in e in the boxed region of interest positioned 200 μ m away from the root tip. g, dwf4 seedlings exhibited an increased CSA uptake capacity. The bioorthogonal reaction was done in 6-d-old Arabidopsis seedlings of Col-0 and dwf4. h, Quantification of fluorescence intensity of images in g in the boxed region of interest positioned 200 μ m away from the root tip. Horizontal and error bars (b,f and h) represent the means and s.d., respectively. n, number of roots (b,f and h). The significant differences were determined with ANOVA and Tukey's multiple comparison tests. ***P < 0.001 and **P < 0.01 for b,f and h. Scale bars, 100 μ m (e and g). For a and b, experiments were performed in four repeats with similar results; for c-f, in three repeats; and for g and h, in two repeats with similar results.

fact that the molecules that negatively regulate BR signaling⁴³ are also transported via PD. Additionally, changes in the cell wall composition of PD mutants might trigger BR signaling without the ligand binding⁴⁴

and mask reduced hormone synthesis. Whether the BR biosynthetic machinery is associated with PD and what physiological relevance this association might have remained to be tested in detail in future studies.



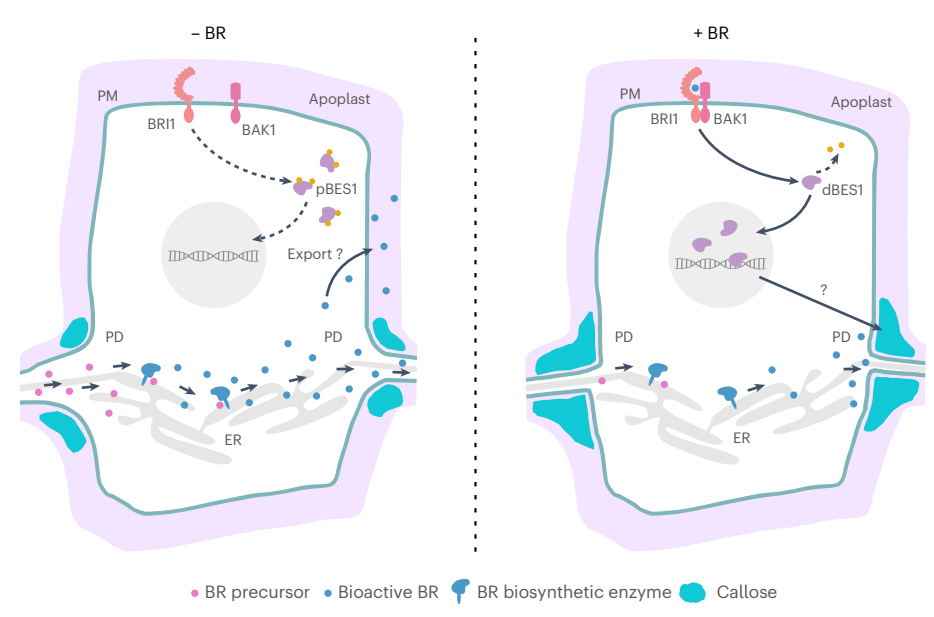


Fig. 5 | **PD-mediated transport and homeostasis of BR biosynthesis and signaling.** BR biosynthetic enzymes are expressed in neighboring cells, requiring the exchange of BR intermediates through PD to produce bioactive BRs. Once synthesized, BRs exit the cell via an unknown mechanism and reach the apoplast (left panel). Once in the extracellular matrix, bioactive BRs bind to the BRI1 receptor and coreceptor BAK1 and initiate a signaling cascade that leads to

dephosphorylation of the BES1 transcription factor. BES1 can then enter the nucleus and initiate transcriptional responses. High levels of BRs increase callose deposition and decrease PD permeability, possibly via BR signaling-initiated transcriptional regulation. Restricted BR precursor movements reduce hormone production and contribute to optimal BR signaling level maintenance (right panel). PM, plasma membrane; PD, plasmodesmata; ER, endoplasmic reticulum.

To further demonstrate the PD-mediated BR movement, we used precursor feeding experiments. Conditionally disrupting cell-to-cell communication, specifically in the endodermis, prevented the rescue of dwf4 mutants with their exogenous product, 22-OHCR. Hence, we concluded that closed PD in mid-positioned root cell files blocks this BR precursor movement and prevents it from reaching inner tissues where it can be converted to downstream BR precursors. Nevertheless, it seems that the transport of 22-OHCR was not completely blocked by the PD constriction, leaving the possibility for partial apoplastic movement of the hormone. Currently, no tools are available that allow monitoring of the BR distribution or movement in plant tissues, in contrast to other plant hormones⁴⁵, Alexa Fluor 647-CS (AFCS) is the only existing bioactive fluorescently labeled BR that could be used to track BR movements in living cells⁴⁶, but this chemical probe might be problematic because of the bulky fluorophore. Therefore, we took a bioorthogonal chemistry approach and developed the BR probe CSA that can be visualized with confocal microscopy after conjugation with an azide-BDP-FL probe. Click chemistry allowed us to follow the CSA distribution in *Arabidopsis* roots under perturbed PD permeability conditions. When the endodermal PD were closed, CSA accumulated in epidermal and cortical cells and could not reach the stele, but when PD were blocked in the epidermis, the CSA was detected only in epidermal cells. This interesting finding implies that only epidermal cells of the root can directly uptake BRs and possibly other steroid-like compounds frequently used in plant research, such as EST. In addition, plants with an enhanced PD permeability accumulated more CSA in all cell files of the root. Together, these results demonstrate that the PD play a crucial role in short-distance BR transport.

Maintenance and regulation of BR levels in cells are essential for plant growth and development. The feedback transcriptional regulation of key BR biosynthetic genes by direct BES1 and BZR1 binding to their promoters is one of the well-known mechanisms for retaining BR homeostasis⁵. Intriguingly, in *Arabidopsis* roots, the expression domains of BR biosynthetic enzymes are separated. We hypothesize that this spatial organization of the biosynthetic pathway allows more

flexible control of hormone biosynthesis through precursor transport regulation. Indeed, the callose immunostaining together with click chemistry-based visualization of BRs revealed that intracellular BR content, probably through BR signaling, regulates PD permeability. Presumably, control of the callose-regulating turnover, and, hence, BR mobility, can optimize BR biosynthesis and signaling, thus creating a negative feedback regulation loop between PD permeability and intracellular BR content. Nevertheless, how BR signaling impacts callose production and degradation at PD remains to be investigated. Recently, the callose synthase gene, glucan synthase-like 8 with a function in plant defense, has been reported as a direct target of BES1, and its expression to be induced by BRs⁴⁷. Our analysis of existing BR response single-cell RNA-sequencing datasets³⁶ revealed that two other genes implicated in callose turnover regulation in the Arabidopsis root, PDLP3 (ref. 48) and GSL4 (ref. 49), are upregulated after BR treatment.

Collectively, our results show that BR precursors are transported through PD after their biosynthesis in the PD-neighboring ER membrane to complete BR biosynthesis and to produce bioactive BRs (Fig. 5). In turn, elevated BR levels can alter callose deposition and decrease PD permeability, possibly through transcriptional regulation initiated by BR signaling, thereby reducing hormone production by restricting the movement of BR precursors. In contrast, low intracellular BR levels lead to decreased callose deposition and increased PD permeability, with enhanced hormone production as a consequence. This negative feedback loop ensures the precise amount of bioactive BRs that is beneficial to plant growth and development. Our work reveals a thus far unknown BR transport pathway in plants and expands the regulatory mechanisms of hormone homeostasis.

Online content

Any methods, additional references, Nature Portfolio reporting summaries, source data, extended data, supplementary information, acknowledgements, peer review information; details of author contributions and competing interests; and statements of data and code availability are available at https://doi.org/10.1038/s41589-023-01346-x.

References

- Nolan, T. M., Vukašinović, N., Liu, D., Russinova, E. & Yin, Y. Brassinosteroids: multidimensional regulators of plant growth, development, and stress responses. *Plant Cell* 32, 295–318 (2020).
- Yin, Y. et al. BES1 accumulates in the nucleus in response to brassinosteroids to regulate gene expression and promote stem elongation. Cell 109, 181–191 (2002).
- Wang, Z.-Y. et al. Nuclear-localized BZR1 mediates brassinosteroid-induced growth and feedback suppression of brassinosteroid biosynthesis. Dev. Cell 2, 505–513 (2002).
- Anfang, M. & Shani, E. Transport mechanisms of plant hormones. Curr. Opin. Plant Biol. 63, 102055 (2021).
- He, J.-X. et al. BZR1 is a transcriptional repressor with dual roles in brassinosteroid homeostasis and growth responses. Science 307, 1634–1638 (2005).
- Vukašinović, N. et al. Local brassinosteroid biosynthesis enables optimal root growth. Nat. Plants 7, 619–632 (2021).
- 7. Clouse, S. D. Brassinosteroids. *Arabidopsis Book* **9**, e0151 (2011).
- 8. Park, J. W., Reed, J. R., Brignac-Huber, L. M. & Backes, W. L. Cytochrome P450 system proteins reside in different regions of the endoplasmic reticulum. *Biochem. J.* **464**, 241–249 (2014).
- Kim, H. B. et al. The regulation of DWARF4 expression is likely a critical mechanism in maintaining the homeostasis of bioactive brassinosteroids in Arabidopsis. Plant Physiol. 140, 548–557 (2006).
- Northey, J. G. B. et al. Farnesylation mediates brassinosteroid biosynthesis to regulate abscisic acid responses. *Nat. Plants* 2, 16114 (2016).
- Contrò, V., R. Basile, J. & Proia, P. Sex steroid hormone receptors, their ligands, and nuclear and non-nuclear pathways. AIMS Mol. Sci. 2, 294–310 (2015).
- Symons, G. M. & Reid, J. B. Brassinosteroids do not undergo long-distance transport in pea. Implications for the regulation of endogenous brassinosteroid levels. *Plant Physiol.* 135, 2196–2206 (2004).
- Faulkner, C. Plasmodesmata and the symplast. Curr. Biol. 28, R1374–R1378 (2018).
- Thomas, C. L., Bayer, E. M., Ritzenthaler, C., Fernandez-Calvino, L. & Maule, A. J. Specific targeting of a plasmodesmal protein affecting cell-to-cell communication. *PLoS Biol.* 6, e7 (2008).
- Lucas, W. J. et al. Selective trafficking of KNOTTED1 homeodomain protein and its mRNA through plasmodesmata. Science 270, 1980–1983 (2016).
- Lucas, W. J. & Lee, J.-Y. Plasmodesmata as a supracellular control network in plants. Nat. Rev. Mol. Cell Biol. 5, 712–726 (2004).
- Feng, Z. et al. The ER-membrane transport system is critical for intercellular trafficking of the NSm movement protein and tomato spotted wilt tospovirus. *PLoS Pathog.* 12, e1005443 (2016).
- Lazarowitz, S. G. & Beachy, R. N. Viral movement proteins as probes for intracellular and intercellular trafficking in plants. *Plant Cell* 11, 535–548 (1999).
- Chitwood, D. H. & Timmermans, M. C. P. Small RNAs are on the move. *Nature* 467, 415–419 (2010).
- Sager, R. E. & Lee, J.-Y. Plasmodesmata at a glance. J. Cell Sci. 131, jcs209346 (2018).
- Yan, D. et al. Sphingolipid biosynthesis modulates plasmodesmal ultrastructure and phloem unloading. *Nat. Plants* 5, 604–615 (2019).
- Burch-Smith, T. M. & Zambryski, P. C. Loss of INCREASED SIZE EXCLUSION LIMIT (ISE)1 or ISE2 increases the formation of secondary plasmodesmata. Curr. Biol. 20, 989–993 (2010).
- 23. Ro, D. K., Mah, N., Ellis, B. E. & Douglas, C. J. Functional characterization and subcellular localization of poplar (*Populus trichocarpa x Populus deltoides*) cinnamate 4-hydroxylase. *Plant Physiol.* **126**, 317–329 (2001).

- Silvestro, D., Andersen, T. G., Schaller, H. & Jensen, P. E. Plant sterol metabolism. Δ7-sterol-C5-desaturase (STE1/DWARF7), Δ5,7-sterol-Δ7-reductase (DWARF5) and Δ24-sterol-Δ24-reductase (DIMINUTO/DWARF1) show multiple subcellular localizations in Arabidopsis thaliana (Heynh) L. PLoS One 8, e56429 (2013).
- Grison, M. S., Petit, J. D., Glavier, M. & Bayer, E. M. Quantification of protein enrichment at plasmodesmata. *Bio Protoc.* 10, e3545 (2020).
- Brault, M. L. et al. Multiple C2 domains and transmembrane region proteins (MCTPs) tether membranes at plasmodesmata. *EMBO Rep.* 20, e47182 (2019).
- 27. Wu, S. et al. Symplastic signaling instructs cell division, cell expansion, and cell polarity in the ground tissue of *Arabidopsis thaliana* roots. *Proc. Natl Acad. Sci. USA* **113**, 11621–11626 (2016).
- Wang, Y. et al. Strigolactone/MAX2-induced degradation of brassinosteroid transcriptional effector BES1 regulates shoot branching. Dev. Cell 27, 681–688 (2013).
- Lee, J.-Y. et al. A plasmodesmata-localized protein mediates crosstalk between cell-to-cell communication and innate immunity in *Arabidopsis*. *Plant Cell* 23, 3353–3373 (2011).
- Benitez-Alfonso, Y. et al. Symplastic intercellular connectivity regulates lateral root patterning. Dev. Cell 26, 136–147 (2013).
- 31. Hacham, Y. et al. Brassinosteroid perception in the epidermis controls root meristem size. *Development* **138**, 839–848 (2011).
- 32. Jao, C. Y. et al. Bioorthogonal probes for imaging sterols in cells. *ChemBioChem* **16**, 611–617 (2015).
- Lee, M. & Schiefelbein, J. WEREWOLF, a MYB-related protein in Arabidopsis, is a position-dependent regulator of epidermal cell patterning. Cell 99, 473–483 (1999).
- 34. Gerlitz, N., Gerum, R., Sauer, N. & Stadler, R. Photoinducible DRONPA-s: a new tool for investigating cell-cell connectivity. *Plant J.* **94**, 751–766 (2018).
- 35. De Rybel, B. et al. Chemical inhibition of a subset of *Arabidopsis thaliana* GSK3-like kinases activates brassinosteroid signaling. *Chem. Biol.* **16**, 594–604 (2009).
- Nolan, T. M. et al. Brassinosteroid gene regulatory networks at cellular resolution in the *Arabidopsis* root. *Science* 379, eadf4721 (2023).
- Tarkowska, D. & Strnad, M. Isoprenoid-derived plant signaling molecules: biosynthesis and biological importance. *Planta* 247, 1051–1066 (2018).
- 38. Lindsey, K., Pullen, M. L. & Topping, J. F. Importance of plant sterols in pattern formation and hormone signalling. *Trends Plant Sci.* **8**, 521–525 (2003).
- Fujioka, S. & Yokota, T. Biosynthesis and metabolism of brassinosteroids. Annu. Rev. Plant Biol. 54, 137–164 (2003).
- 40. Caño-Delgado, A. et al. BRL1 and BRL3 are novel brassinosteroid receptors that function in vascular differentiation in *Arabidopsis*. *Development* **131**, 5341–5351 (2004).
- Yamanaka, N., Marqués, G. & O'Connor, M. B. Vesicle-mediated steroid hormone secretion in *Drosophila melanogaster*. Cell 163, 907–919 (2015).
- 42. Atkovska, K., Klingler, J., Oberwinkler, J., Keller, S. & Hub, J. S. Rationalizing steroid interactions with lipid membranes: conformations, partitioning, and kinetics. ACS Cent. Sci. 4, 1155–1165 (2018).
- 43. Band, L. R. Auxin fluxes through plasmodesmata. *New Phytol.* **231**, 1686–1692 (2021).
- 44. Wolf, S., Mravec, J., Greiner, S., Mouille, G. & Höfte, H. Plant cell wall homeostasis is mediated by brassinosteroid feedback signaling. *Curr. Biol.* **22**, 1732–1737 (2012).
- 45. Isoda, R. et al. Sensors for the quantification, localization and analysis of the dynamics of plant hormones. *Plant J.* **105**, 542–557 (2021).

- Irani, N. G. et al. Fluorescent castasterone reveals BRI1 signaling from the plasma membrane. Nat. Chem. Biol. 8, 583–589 (2012).
- Xiong, J. et al. Brassinosteroids positively regulate plant immunity via BRI1-EMS-SUPPRESSOR 1-mediated GLUCAN SYNTHASE-LIKE 8 transcription. Front. Plant Sci. 13, 854899 (2022).
- 48. Mehra, P. et al. Hydraulic flux-responsive hormone redistribution determines root branching. *Science* **378**, 762–768 (2022).
- 49. Liu, J., Liu, Y., Wang, S., Cui, Y. & Yan, D. Heat stress reduces root meristem size via induction of plasmodesmal callose accumulation inhibiting phloem unloading in *Arabidopsis*. *Int. J. Mol. Sci.* **23**, 2063 (2022).

Publisher's note Springer Nature remains neutral with regard to jurisdictional claims in published maps and institutional affiliations.

Springer Nature or its licensor (e.g. a society or other partner) holds exclusive rights to this article under a publishing agreement with the author(s) or other rightsholder(s); author self-archiving of the accepted manuscript version of this article is solely governed by the terms of such publishing agreement and applicable law.

© The Author(s), under exclusive licence to Springer Nature America, Inc. 2023

Methods

Plant materials and growth conditions

The *A. thaliana* (L.) Heynh., accession Col-0, was used in all experiments. Seeds were surface-sterilized with sterilization buffer (80% (vol/vol) ethanol and 20% (vol/vol) sodium hypochlorite), stratified for 2 d in the dark at 4 °C and grown vertically on half-strength Murashige and Skoog (1/2 MS) medium (1%) agar (wt/vol) plates supplemented with 1% (wt/vol) sucrose at 22 °C, with a 16-h light/8-h dark photoperiod. The following mutant lines were used: *dwf4-102* (ref. 50), *cpd*⁶¹, *pDWF4:DWF4-GFP/dwf4* (ref. 6), *pROT3:ROT3-GFP/rot3* (ref. 6), *pCPD:CPD-GFP/cpd*⁶, *pBR6OX2:BR6OX2-GFP/br6ox1;br6ox2* (ref. 6), *pBES1:gBES1-GFP/*Col-0 (ref. 6), *pEN7:icals3m/*Col-0 (ref. 27) and *p35S:PdBG1-mCitrine/*Col-0 (ref. 30). Primers used for genotyping are listed in Supplementary Table 2. The lines *pEN7:icals3m/dwf4* and *pBES1:gBES1-GFP/pEN7:icals3m/dwf4* were obtained by crossing *pEN7:icals3m* with *dwf4-102* and *pEN7:icals3m/dwf4* with *pBES1:gBES1-GFP/*Col-0, respectively.

Plasmid construction and generation of transgenic lines

To generate the p35S:C4H-mCherry and pUBQ10:PDLP1-mCherry constructs, the genomic fragments of C4H (AT2G30490) and PDLP1 (AT5G43980) were amplified by PCR and cloned into pDONR221 (Thermo Fisher Scientific). The resulting entry clones were recombined with the cauliflower mosaic virus 35S and the UBIQUITIN10 promoters in pDNORP4-P1R with pDNORP2R-P3-mCherry for C4H and PDLP1, respectively into the pH7m34GW⁵² destination vector by anLR reaction. The resulting constructs were used for transient expression in tobacco and generation of transgenic plants by introducing them into pDWF4:DWF4-GFP/dwf4 and pROT3:ROT3-GFP/rot3 plants by Agrobacterium tumefaciens-mediated transformation according to the floral dip protocol⁵³. To generate pWER:icals3m, pDONRP4-P1R-WER (obtained from NASC set 2106366) was recombined with icals3m in pDONRP1-P2 and without in pDONRP2R-P3 into the pB7m34GW52 destination vector by an LR reaction. The construct was transformed into Col-0. To generate pCPD:PDLP5-BFP/pCPD:CPD-GFP/cpd and pCPD:PDLP5-BFP/pSCR:CPD-mCherry/cpd lines, the genomic fragment of PDLP5 was cloned into pDONR221 and combined in an LR reaction with pDONRP4-P1R-CPD⁶ and pDNORP2rP3-BFP in the destination vector PK8m34GW-FAST. The resulting constructs were introduced into pCPD:CPD-GFP/cpd⁶ and pSCR:CPD-mCherry/cpd⁶ translational lines. To generate p35S:DWF4-GFP and p35S:ROT3-GFP constructs. the entry clones pDONR221-DWF4 and pDONR221-ROT3 (ref. 6) were put into the pK7FWG2 destination vector by an LR reaction. To generate p35S:MCTP3-GFP construct, MCTP3 (AT3G57880) was amplified by PCR and cloned into pDONR221 (Thermo Fisher Scientific). The resulting entry clone was put into the *pK7FWG2* destination vector by an LR reaction. The cloning primers are listed in Supplementary Table 2.

Chemical treatments

BL (OlChemIm), BRZ (Tokyo Chemical Industry), β -EST (EST; Sigma-Aldrich), BIK (Sigma-Aldrich), 22-OHCR and CSA were kept at different stock concentrations in dimethyl sulfoxide (DMSO) and were diluted 1,000× to reach the final concentrations in the media. For the mock treatment, DMSO was at a final concentration of 0.1% (vol/vol). Specific treatments are described in the main text and/or figure legends.

Immunoblot analysis

For the BES1 immunoblot analysis of *pEN7:icals3m* seedlings, the experiments were done in triplicate. Five-day-old Col-0 and *pEN7:icals3m* seedlings were transferred to fresh 1/2 MS medium agar plates containing DMSO or 5 µM EST. The root tips were collected for immunoblotting after 12 h of treatment. For the BES1 immunoblot analysis of *pCPD:PDLP5-BFP/pCPD:CPD-GFP/cpd* and *pCPD:PDLP5-BFP/pSCR:CPD-mCherry/cpd* lines, the experiments were done in

triplicate. Six-day-old seedlings (root part) were collected for the BES1 assay. For the p35S:PdBG1-mCitrine line, experiments were done in duplicate. Six-day-old seedlings of p35S:PdBG1-mCitrine and Col-0 were collected for the BES1 assay. For the 22-OHCR activity tests, experiments were done in duplicate. Five-day-old Col-0. dwf4 and cpd seedlings were transferred to 1/2 MS medium agar plates containing DMSO, BL (500 pM) or 22-OHCR (500 nM) for 24 h and collected for the BES1 assay. For the CSA activity test, experiments were done in duplicate. Five-day-old dwf4 seedlings were transferred to fresh 1/2 MS medium agar plates containing DMSO, CS (1 µM and 10 µM) or CSA (1 μM and 10 μM) and collected after 24 h for the BES1 assay. All plant material was frozen in liquid nitrogen, ground by Retsch MM400 and homogenized in 100 µl of ice-cold homogenization buffer (1% (vol/ vol) SDS, 25 mM Tris-HCl, pH 7.5, 150 mM NaCl, 10 mM dithiothreitol and Roche Complete protease inhibitor (one tablet/10 ml)) and placed on ice for 30 min. The homogenates were centrifuged twice (10 min, 20,000g) at 4 °C. After the addition of 4× lithium dodecyl sulfate and sample-reducing agent (10×), the samples were heated for 10 min at 70 °C, centrifuged again, separated on 4-15% (vol/vol) SDS-polyacrylamide gel electrophoresis stain-free protein gel (Bio-Rad Laboratories) and blotted on Trans-Blot Turbo Mini PVDF Transfer Packs. Membranes were blocked at 4 °C in 5% (vol/vol) skimmed milk (Difco). For immunodetection, the anti-BES1 antibody at 1:5,000 was used as the primary antibody and donkey anti-rabbit (Merck) at 1:10,000 as the secondary antibody. For tubulin detection, the anti-tubulin (Abcam) at 1:5,000 was used as the primary antibody and the sheep anti-mouse (Merck) at 1:10,000 as the secondary antibody. Proteins were detected by the ChemiDoc MP Imaging System (Bio-Rad Laboratories). For the BES1 dephosphorylation assay, the ratio of dBES1 to total BES1 proteins was quantified according to the signal intensity. Loading was adjusted to an equal level based on the amount of tubulin. Signal intensities were determined with Image Lab (Bio-Rad Laboratories).

Synthesis of chemical compounds and bioorthogonal chemistry

CSA and 22-OHCR were synthesized as described (Supplementary Notes 1 and 2). Azide–BDP–FL (Jena Bioscience, CLK-044-1) and Click-&-Go Cell Reaction Buffer Kit (Click Chemistry Tools, 1263) were used for click chemistry labeling experiments. The plant material was incubated without or with CSA (20 μ M) in liquid 1/2 MS medium for 4 h, washed twice with PBS, fixed with 3.7% (vol/vol) formaldehyde in PBS for 15 min and washed twice with 3% (wt/vol) BSA in PBS. The samples were permeabilized by 0.5% (vol/vol) Triton X-100 in PBS for 20 min at room temperature and washed three times with 3% (wt/vol) BSA in PBS. The click chemistry was done according to the manufacturer's instructions (Click Chemistry Tools), using Azide–BDP–FL at a 4 μ M concentration in the reaction mixture for 30 min. Samples were washed with 3% (wt/vol) BSA in PBS, counterstained by propidium iodide (PI) at 1:1,000 dilution in H_2O and imaged.

Aniline blue staining

Seedlings were fixed and destained in 1:3 acetic acid/ethanol until the material was transparent (usually 2 h), then washed in 150 mM $\rm K_2HPO_4$ for 30 min. Next, seedlings were incubated for at least 4 h in 150 mM $\rm K_2HPO_4$ and 0.01% (wt/vol) aniline blue (staining solution) in tubes wrapped in aluminum foil for light protection, washed in 150 mM $\rm K_2HPO_4$ for 5 min and imaged.

Callose immunostaining

Arabidopsis seedlings were vertically grown on 1/2 MS medium agar plates for 4 d, then transferred to fresh media with the following treatments for another 24 h: 200 nM BR, 1 μ M BRZ and DMSO mock. The immunolocalization procedure was done according to the published protocol ⁵⁴. In summary, seedlings were fixed in 4% (vol/vol) paraformal-dehyde in microtubule stabilization buffer [MTSB; 50 mM piperazine-

N,N'-bis(2-ethanesulfonicacid), $5\,\mathrm{mM}$ (ethyleneglycol-bis(β -aminoethyl ether)-N,N,N',N'-tetraacetic acid, $5\,\mathrm{mM}$ MgSO₄, pH 7 with KOH]. Root tips were cut and mounted on poly-lysine-coated microscopy slides. Unspecific binding was prevented by blocking in neutral donkey serum before incubation with the antibody. The callose antibody (Australia Biosupplies) was diluted to 1:500 in MTSB containing 5% (vol/vol) neutral donkey serum and incubated with the samples for $4\,\mathrm{h}$ at room temperature. The secondary goat anti-mouse IgG (H&L)—Alexa Fluor $594\,\mathrm{was}$ diluted to 1:500 in MTSB buffer containing 5% (vol/vol) neutral donkey serum and incubated with the samples for $1\,\mathrm{h}$.

Reverse transcription-quantitative PCR

Total RNA was extracted by reverse transcription—quantitative PCR from 6-d-old seedlings with the RNeasy Mini Kit (Qiagen). Genomic DNA was eliminated by on-column digestion with RQ1 RNase-free DNase (Promega) during the isolation procedure. cDNA was generated from 1 µg of total RNA with qScript cDNA SuperMix (Quantabio) and analyzed on a LightCycler 48 II apparatus (Roche) with the SYBR Green I Master mix (Roche) according to the manufacturer's instructions. Expression levels were normalized to those of ACTIN2. Primers are listed in Supplementary Table 2.

Analysis of BL scRNA-seq

To examine the transcriptional regulation of PD-related genes by BRs, we reanalyzed a previously described scRNA-seq dataset (GEO: GSE212230) in which wild-type *Arabidopsis* plants were grown on 1 µM BRZ for 7 d and transferred to 1 µM BRZ versus 100 nM BL for 2 h (ref. 36). First, we constructed a heatmap by calculating the log₂ fold-change of BL 2 h/BRZ using aggregated counts across all cell types and developmental stages. The heatmap was visualized with ComplexHeatmap (v2.10.0)⁵⁵. Differentially expressed genes from each combination of cell type and developmental stage of the root³⁶ were used to identify BL-regulated PD-related genes. We then plotted the log-normalized, 'corrected' counts produced by the SCTransform function ⁵⁶ for *PDLP3* and *CalS8/GSL4* on the two-dimensional uniform manifold approximation and projection embedding.

Microscopy and image analysis

Most of the images were captured by a Leica SP8X confocal microscope. Images were collected using Las-X software (v 3.5.0.18371). GFP and mCherry were excited at 488 nm and 594 nm and acquired at 500-530 nm and at 600-650 nm, respectively. For the study of subcellular localization of BR biosynthetic enzymes, images were taken by a ×40/1.10 WATER objective and signal accumulation was used during $confocal\ imaging\ for\ \textit{Arabidopsis}\ lines\ related\ to\ ROT3\ and\ DWF4.\ For$ the experiments related to the transgenic line pBES1:gBES1-GFP, Arabidopsis roots were mounted in a PI (Sigma-Aldrich) (10 ng ml⁻¹) solution between slides and coverslips and images were taken by a ×25/0.95 WATER objective. Nine cells from the root transition zone were used for BES1-GFP signal quantification. For the click chemistry experiments, the BDP-FL signal was detected with a 503-nm laser excitation and a 505- to 519-nm emission filter, and images were taken by a ×25/0.95 WATER objective. For pDWF4:DWF4-GFP/pUBI10:PDLP1-mCherry and pROT3:ROT3-GFP/pUBI10:PDLP1-mCherry in Extended Data Fig. 1g, roots were imaged under a vertical Zeiss LSM 900 microscope equipped with a Plan-Apochromat M27 20×/0.8 n.a. objective. GFP and mCherry were excited at 488 and 587 nm and acquired at 410-546 nm and at 595–700 nm, respectively. For immunostaining, samples were imaged with a Zeiss LSM 880 microscope with an ×40/NA 1.3 oil lens. Atto550 excitation was done with 0.3% of 561-nm power, and fluorescence was collected between 566 and 700 nm. Zeiss ZEN 3.3 (blue edition) software was used for image collection with Zeiss LSM 880 and Zeiss LSM 900 microscopes. Callose deposition at PD was quantified for whole root meristems with the Fiji software (https://fiji.sc/) macroinstruction program (Supplementary Note 3). The callose signal at the cell plate was excluded from the measurements. The experiment was repeated two times with similar results. For aniline blue staining, a 405-nm laser excitation and a 505-nm long-pass emission filter were used for imaging. Image analysis was done with the Fiji software. To measure the length of mature cortical cells, seedlings were stained with PI (Sigma-Aldrich) and images were taken with $\times 25/0.95$ WATER objective. The cells from the root region, in which root hairs start to emerge (a sign of cell differentiation after cessation of elongation), were imaged and measured.

Two-photon microscopy and cell diffusion assay with DRONPA-s

Five-day-old 35S-DRONPA-s seedlings were grown on 1/2 MS agar plates under long-day conditions at 21 °C and 70% humidity. Then, they were transferred to plates containing either DMSO or 200 nM BL for an additional 24 h. Before imaging, plants were incubated for 2 min in 1/500 PI in a water solution. In total, 15-20 roots were analyzed with two to three regions of interest (ROIs) per root. For the DRONPA-s assay, root tips were analyzed with a Leica TCS SP5-multiphoton confocal microscope set up. PI was excited at 488 nm and detected at 620-700 nm. Fluorescence intensities were quantified with the Leica LAS AF software. For DRONPA-s deactivation, root tips were illuminated with 488-nm light for 45 s at 70% of the total laser intensity (argon laser, 20 mW; Leica Microsystems). For DRONPA-s activation, three ROIs (corresponding to three cells per root) were set to the center of the cell to avoid activation of the adjacent cells. ROIs were illuminated with 800-nm light for 5 s using a two-photon infrared (IR) (Titane-Saphir pulsating laser). Laser power is circa 2.6 W with a 20% gain. For DRONPA-s acquisition, the detection was made 2 s after single-cell activation up to 120 s, with 20% (488 nm) argon laser at emission 500-575 nm. For DRONPA-s movement analysis, mean fluorescence intensities were measured from the activated cell and the two adjacent cells in ImageJ. DRONPA-s movement was calculated as a fluorescent signal moving from the activated cell into the adjacent cells. X-Y drifts were corrected with the StackReg plugin. After normalization and background subtraction, values were transformed into percentages of the average fluorescence from the two adjacent cells. The activated cell is considered to be at 100% (for example, 100% of the DRONPA-s molecules were activated in the ROI). A total of 15–20 roots were analyzed with two to three ROIs per root.

PD index

PD enrichment was assessed by calculating the fluorescence intensity of FP-tagged DWF4, PD localized MCTP3 and the ER protein HDEL⁵⁷, at (1) PD (indicated by PDLP1-mCherry or PDCB1-mCherry) and (2) the cell periphery. Constructs of interest were transiently co-expressed in N. benthamiana leaves with PDLP1-mCherry or PDCB1-mCherry (PD markers). Confocal images of leaf epidermal cells were acquired by sequential scanning of PDLP1-mCherry or PDCB1-mCherry in channel 1 and GFP/BFP-tagged proteins in channel 2. Approximately 20 images of leaf epidermis cells were acquired for each combination. The quantification was carried out according to the standard protocol²⁵. Individual images were processed using ImageJ by defining six ROIs at PD (using PD marker to define the ROI in channel 1) and 12 ROIs at the cell periphery outside PD. The GFP/BFP-tagged protein mean intensity (channel 2) was measured for each ROI and then averaged for a single image. The PD index corresponds to the intensity ratio between the fluorescence intensity of the protein of interest at PD versus the cell periphery outside of PD. Roots expressing DWF4-GFP/ROT3-GFP and PDLP1-mCherry were imaged in a similar fashion to tobacco leaves, and the PD index for more than 20 cells per transgenic line (four roots per line) was calculated as explained above.

Statistical analysis

All statistical analyses were carried out with GraphPad Prism v.8.0 and v.9.0 software. Two-tailed Student's paired *t*-test was used for

BES1 immunoblot analysis. Comparison of more than two genotypes or treatments was done with a one-way analysis of variance. Tukey's multiple comparison tests were used in the comparison procedure (***P < 0.001, **P < 0.01 and *P < 0.05).

Reporting summary

Further information on research design is available in the Nature Portfolio Reporting Summary linked to this article.

Data availability

Numerical source data files and uncropped scans of blots are provided for figures and extended data figures. Primer lists, Fiji macro for callose deposition quantification and notes on synthesis of chemical compound used in this study can be found in Supplementary Information. Source data are provided with this paper.

Code availability

Single-cell RNA-sequencing data analysis code used in this study is deposited at GitHub at https://github.com/tmnolan/Plasmodesmata-mediate-cell-to-cell-transport-of-brassinosteroid-hormones.

References

- Zhang, R., Xia, X., Lindsey, K. & da Rocha, P. S. C. Functional complementation of dwf4 mutants of Arabidopsis by overexpression of CYP724A1. J. Plant Physiol. 169, 421–428 (2012).
- Szekeres, M. et al. Brassinosteroids rescue the deficiency of CYP90, a cytochrome P450, controlling cell elongation and de-etiolation in Arabidopsis. Cell 85, 171–182 (1996).
- 52. Karimi, M., De Meyer, B. & Hilson, P. Modular cloning in plant cells. *Trends Plant Sci.* **10**, 103–105 (2005).
- 53. Clough, S. J. & Bent, A. F. Floral dip: a simplified method for *Agrobacterium*-mediated transformation of *Arabidopsis thaliana*. *Plant J.* **16**, 735–743 (1998).
- 54. Pendle, A. & Benitez-Alfonso, Y. Immunofluorescence detection of callose deposition around plasmodesmata sites. *Methods Mol. Biol.* **1217**, 95–104 (2015).
- Gu, Z., Eils, R. & Schlesner, M. Complex heatmaps reveal patterns and correlations in multidimensional genomic data. *Bioinformatics* 32, 2847–2849 (2016).
- Hafemeister, C. & Satija, R. Normalization and variance stabilization of single-cell RNA-seq data using regularized negative binomial regression. *Genome Biol.* 20, 296 (2019).
- Coulon, D., Brocard, L., Tuphile, K. & Bréhélin, C. Arabidopsis LDIP protein locates at a confined area within the lipid droplet surface and favors lipid droplet formation. *Biochimie* 169, 29–40 (2020).

Acknowledgements

We thank Y. Benitez-Alfonso (University of Leeds, UK), Y. Helariutta (University of Helsinki, Finland) and L. De Veylder (VIB-Ghent University) for providing published materials; J. Oklestkova (Palacký University, Czech Republic) for the kind gift of castasterone; Q. Yu (VIB-Ghent University) for pUBQ10:PDCB1-mCherry construct; and Y. Yin (Iowa State University, Ames, USA) for providing the anti-BES1 antibody. We thank S. Vanneste (Ghent University, Belgium), M. Strnad

and J. Oklestkova (Palacký University, Czech Republic) for useful discussions and M. De Cock for help in preparing the manuscript. This work was supported by the Research Foundation-Flanders (project G002121N to E.R. and a postdoctoral fellowships 12R7822N and 12R7819N to N.V.), Chinese Scholarship Council (predoctoral fellowships to Y.W.), European Research Council (ERC) under the European Union's Horizon 2020 research and innovation program (project 772103-BRIDGING to E.M.B.), Human Frontier long-term postdoctoral fellowship (LTOO0340/2019 to M.P.P.), ERDF project 'Plants as a tool for sustainable global development' (CZ.02.1.01/ 0.0/0.0/16 019/0000827 to M.K.), National Institute of General Medical Sciences of the National Institutes of Health (R01GM127759 to W.B. and MIRA 1R35GM131725 to P.N.B.), US National Science Foundation (Postdoctoral Research Fellowships in Biology Program IOS-2010686 to T.M.N.), Howard Hughes Medical Institute to P.N.B. as an Investigator, Grants-in-Aid for Scientific Research from the JSPS (JP21H05644 to T.S.) and JSPS Research Fellowship for Young Scientists (to Y.L.). Two-photon cell diffusion assay and root wholemount immunostaining was done on the Bordeaux Imaging Center, member of the national infrastructure France-BioImaging supported by the French National Research Agency (ANR-10-INBS-04).

Author contributions

Y.W., N.V., E.M.B and E.R. initiated the project and designed experiments. Y.W. performed most of the experiments. N.V. prepared constructs and performed imaging. Y.L. performed imaging and calculated the PD index. J.P.S. and M.S. performed callose immunostaining and DRONPA-s imaging and analyzed the data. T.M.N. analyzed scRNA-seq data. M.P.P. generated transgenic lines and contributed materials. B.C. and J.M.W. synthetized CSA, and M.K. and K.F. synthetized 22-OHCR. Y.W., N.V., T.S., E.M.B., W.B., P.N.B. and E.R. analyzed the data and wrote the article. All authors revised the manuscript.

Competing interests

P.N.B. is the cofounder and Chair of the Scientific Advisory Board of Hi Fidelity Technologies, a company that works on crop root growth. The remaining authors declare no competing interests.

Additional information

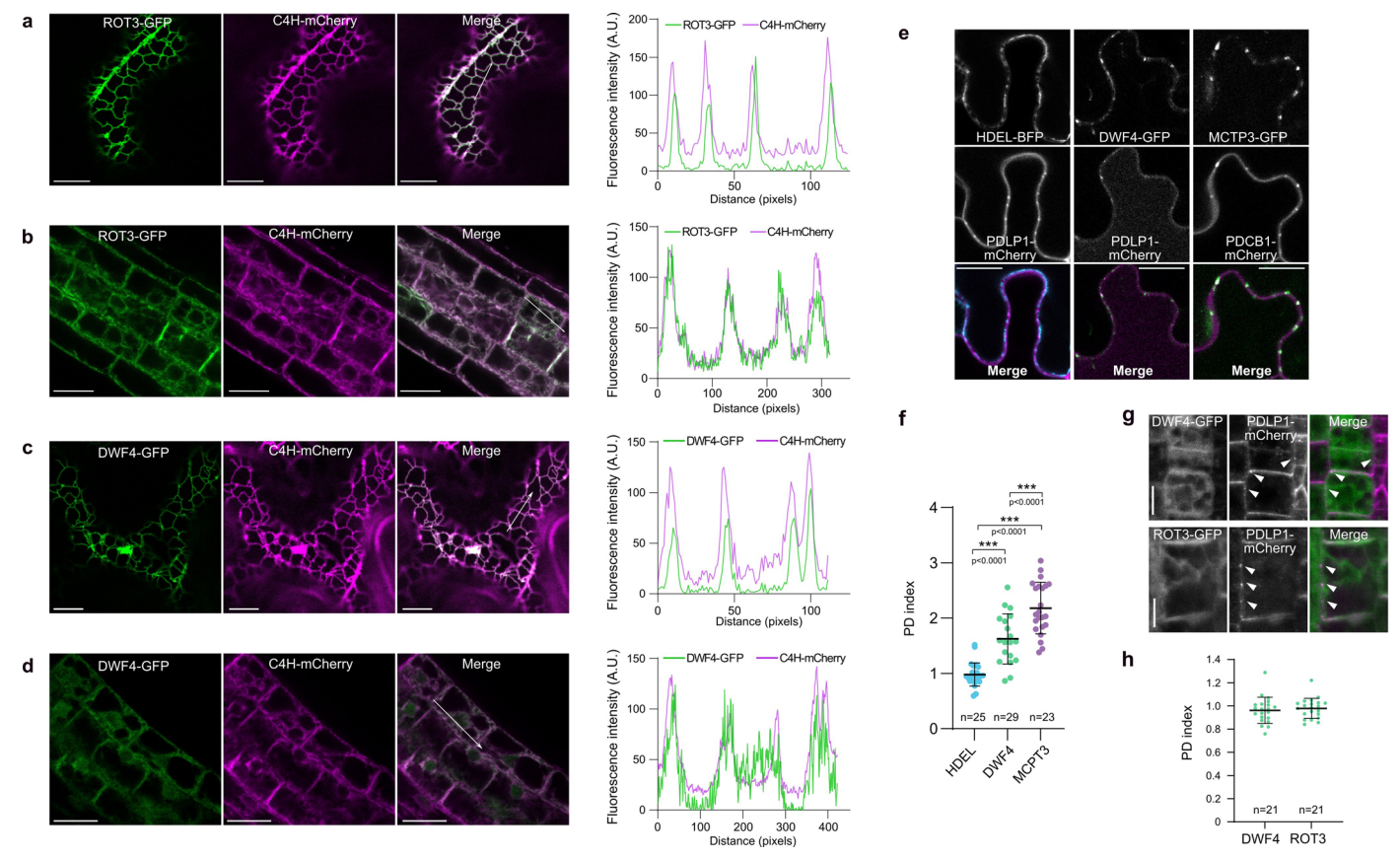
Extended data is available for this paper at https://doi.org/10.1038/s41589-023-01346-x.

Supplementary information The online version contains supplementary material available at https://doi.org/10.1038/s41589-023-01346-x.

Correspondence and requests for materials should be addressed to Nemanja Vukašinović or Eugenia Russinova.

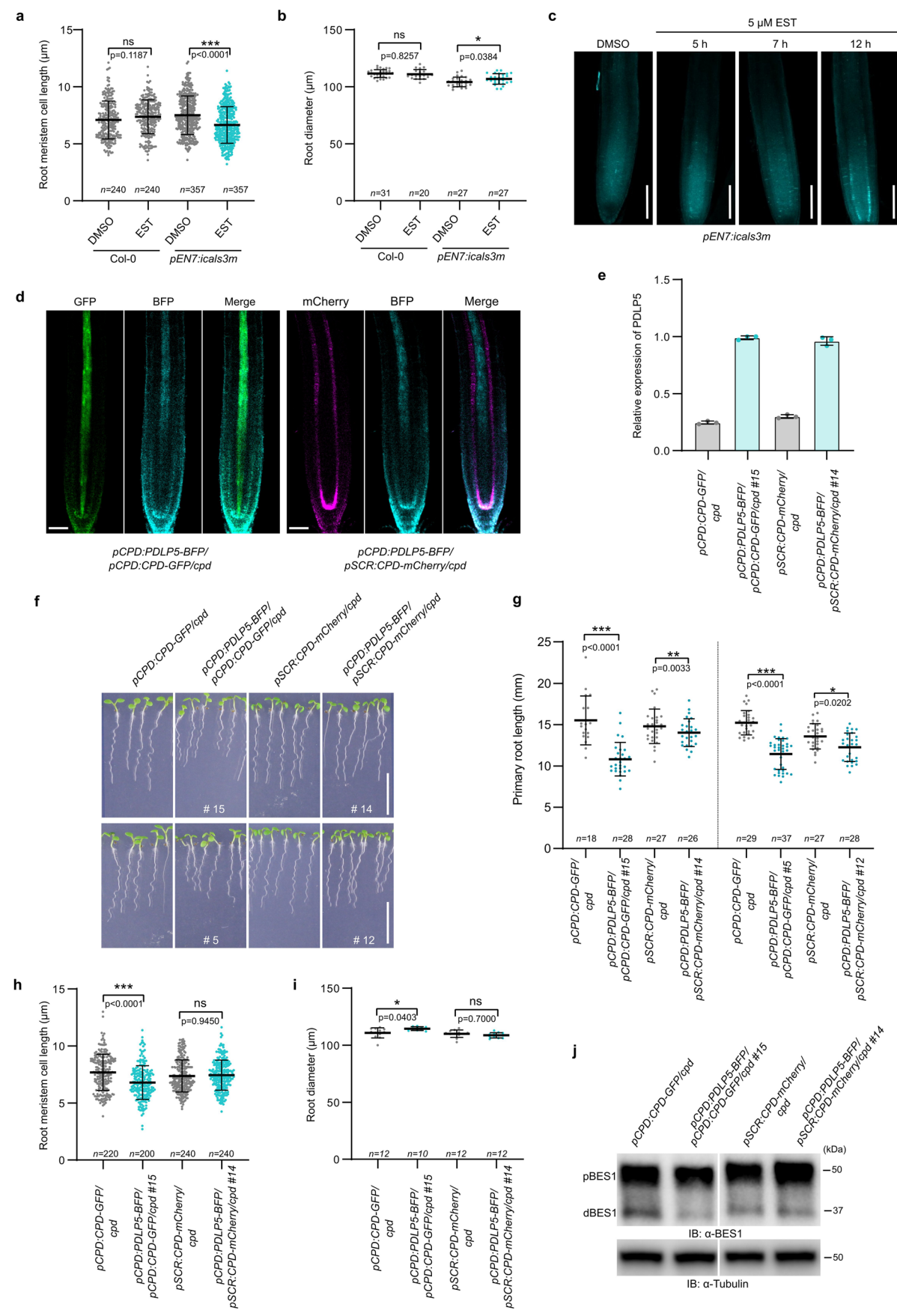
Peer review information *Nature Chemical Biology* thanks Y. Benitez-Alfonso and the other, anonymous, reviewer(s) for their contribution to the peer review of this work.

Reprints and permissions information is available at www.nature.com/reprints.



Extended Data Fig. 1| **Subcellular localization of BR biosynthetic enzymes. a,b,c,d**, The BR biosynthetic enzyme ROT3-GFP and DWF4-GFP co-localize with the ER marker C4H-mCherry when transiently co-expressed in tobacco leaves (**a,c**) and in *Arabidopsis* root epidermal cells expressing ROT3-GFP and DWF4-GFP under the control of their native promoters (**b,d**). The fluorescence intensity profiles along the white arrows are shown on the right. A.U., arbitrary units. **e**, Co-localization of HDEL-BFP and DWF4-GFP with plasmodesmata (PD) marker PDLP1-mCherry and MCTP3-GFP with PD marker PDCB1-mCherry when transiently co-expressed in tobacco leaves. These co-expression combinations were used to calculate PD indexes in (**f**). **f**, The PD index of DWF4-GFP biosynthetic enzyme compared to the indexes of ER marker HDEL-BFP and PD-resident protein MCTP3-GFP. DWF4-GFP index above 1 indicates partial enrichment at PD. All

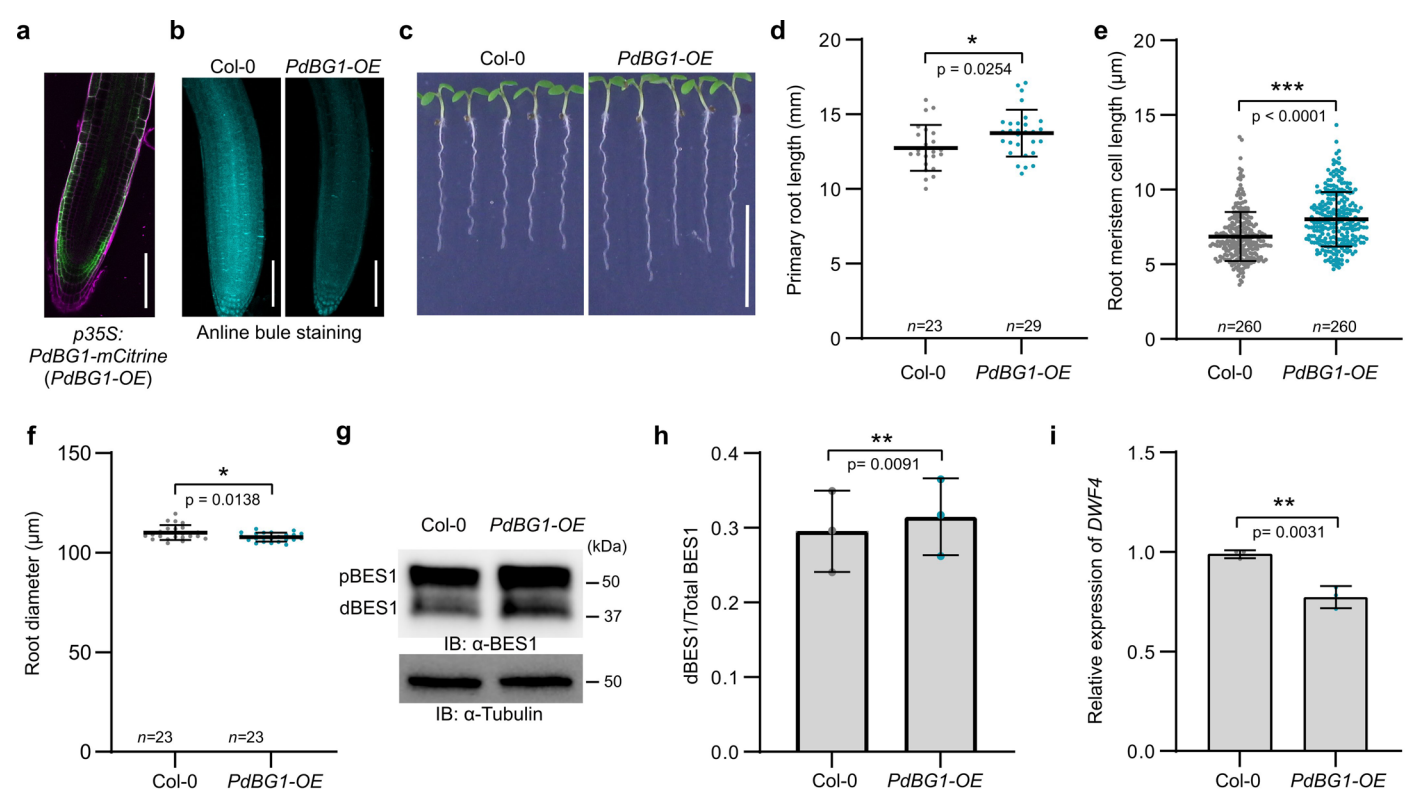
individual data points are plotted. Horizontal and error bars represent the means and s.d., respectively. n, number of ROIs used to calculate average PD index. The significant differences were determined with one-way analysis of variance (ANOVA) and Tukey's multiple comparison tests. *** $P < 0.001\,g$, Co-localization of DWF4-GFP and ROT3-GFP biosynthetic enzymes expressed under their native promoters with the PD marker PDLP1-mCherry in Arabidopsis roots. Epidermal and cortical cells of the root transition zone were imaged for DWF4-GFP and ROT3-GFP, respectively. White arrowheads mark PD, labeled by PDLP1-mCherry. No clear co-localization of BR biosynthetic enzymes and PDLP1-mCherry were observed. Scale bars, $10\,\mu m$ (a,c,g), $20\,\mu m$ (e) and $25\,\mu m$ (b,d). For a,b,c,d,e,f, the experiment was repeated three times and for g,h, twice with similar results.



Extended Data Fig. 2 | See next page for caption.

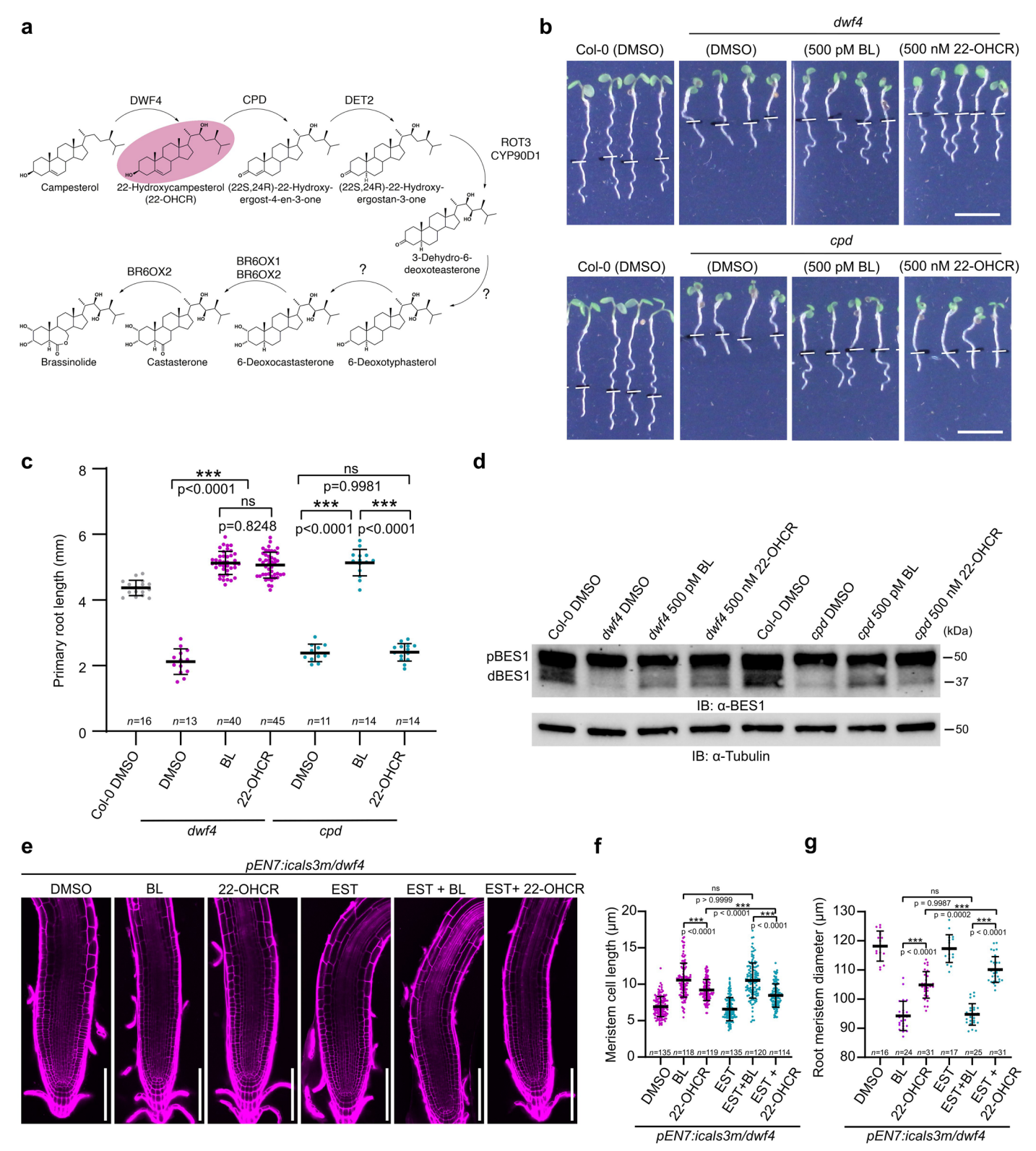
Extended Data Fig. 2 | Reduced cell-to-cell connectivity negatively affects BR signaling. a,b, Quantification of root meristem cell length in (a) and root diameter in (b) of 5-d-old Col-0 and pEN7:icals3m seedlings which were grown for 12 h on agar medium containing either estradiol (EST) (5 μM) or DMSO (mock). For (a,b) the significant differences were determined with two-way analysis of variance (ANOVA) and Šídák's multiple comparisons test. *** P < 0.001 and *P<0.05. c, Aniline blue staining of callose deposition in the root tips of pEN7:icals3m plants. Five-day-old seedlings were transferred to agar medium containing estradiol (EST) (5 µM) for the indicated times and DMSO (mock), followed by aniline blue staining. Scale bars, 100 μm. d, Confocal images of pCPD:PDLP5-BFP/pCPD:CPD-GFP/cpd and pCPD:PDLP5-BFP/pSCR:CPDmCherry/cpd lines. Scale bars, 50 µm. e, The relative gene expression of PDLP5 in pCPD:PDLP5-BFP/pCPD:CPD-GFP/cpd (line #15) and pCPD:PDLP5-BFP/pSCR: CPD-mCherry/cpd (line #14) compared to their segregating siblings that do not express pCPD:PDLP5-BFP. Error bars represent s.d. f, Phenotypes of 6-d-old pCPD:CPD-GFP/cpd, pCPD:PDLP5-BFP/pCPD:CPD-GFP/cpd, pSCR:

CPD-mCherry/cpd, and *pCPD:PDLP5-BFP/pSCR:CPD-mCherry/cpd* seedlings from two independent transgenic lines. For each line, segregating siblings that do not express *pCPD:PDLP5-BFP* are shown. Scale bar, 1 cm. **g**, The quantification of primary root length of transgenic lines shown in (**f**). **h,i**, Quantification of root meristem cell length in (**h**) and root diameter in (**i**) of seedlings shown in (**f**). **j**, Phosphorylation status of BES1 detected by immunoblotting (lB) with α-BES1 antibody in roots. Tubulin detected with α-tubulin antibody was used as loading control. pBES1, phosphorylated BES1, dBES1, dephosphorylated BES1. Two panels from each row are from the same blots and were cropped and arranged for clarity. For **a,b,g,h,i**, all individual data points are plotted. Horizontal and error bars represent the means and s.d., respectively. *n*, number of roots used in **b,g,i**, and cells used in **a,h**. The significant differences for **g,h,i**, were determined with one-way ANOVA and Tukey's multiple comparison tests. *** *P* < 0.001, ** *P* < 0.01, and * *P* < 0.05. For **a,b,h,i,j**, the experiment was repeated twice and for **f,g**, three times with similar results.



Extended Data Fig. 3 | Increased cell-to-cell connectivity positively affects BR signaling. a, A confocal image of 6-d-old p35S:PdBG1-mCitrine (PdBG1-OE) root meristem. Cell walls were stained with propidium iodide. b, Aniline blue staining of callose deposition in the root tips of PdBG1-OE plants. Scale bars, $100 \, \mu m$ (a,b). c, Phenotype of 6-d-old PdBG1-OE seedlings. Scale bar, $1 \, cm$. d,e,f, Quantification of the primary root length (d), root meristem cell length (e) and root meristem diameter (f) shown in (c). All individual data points are plotted. Horizontal and error bars represent the means and s.d., respectively. n, number of roots (d,f) and cells (e). The significant difference was determined with two-tailed Student's unpaired t-test analysis. ***P<0.001, **P<0.01, and *P<0.05. g, Phosphorylation

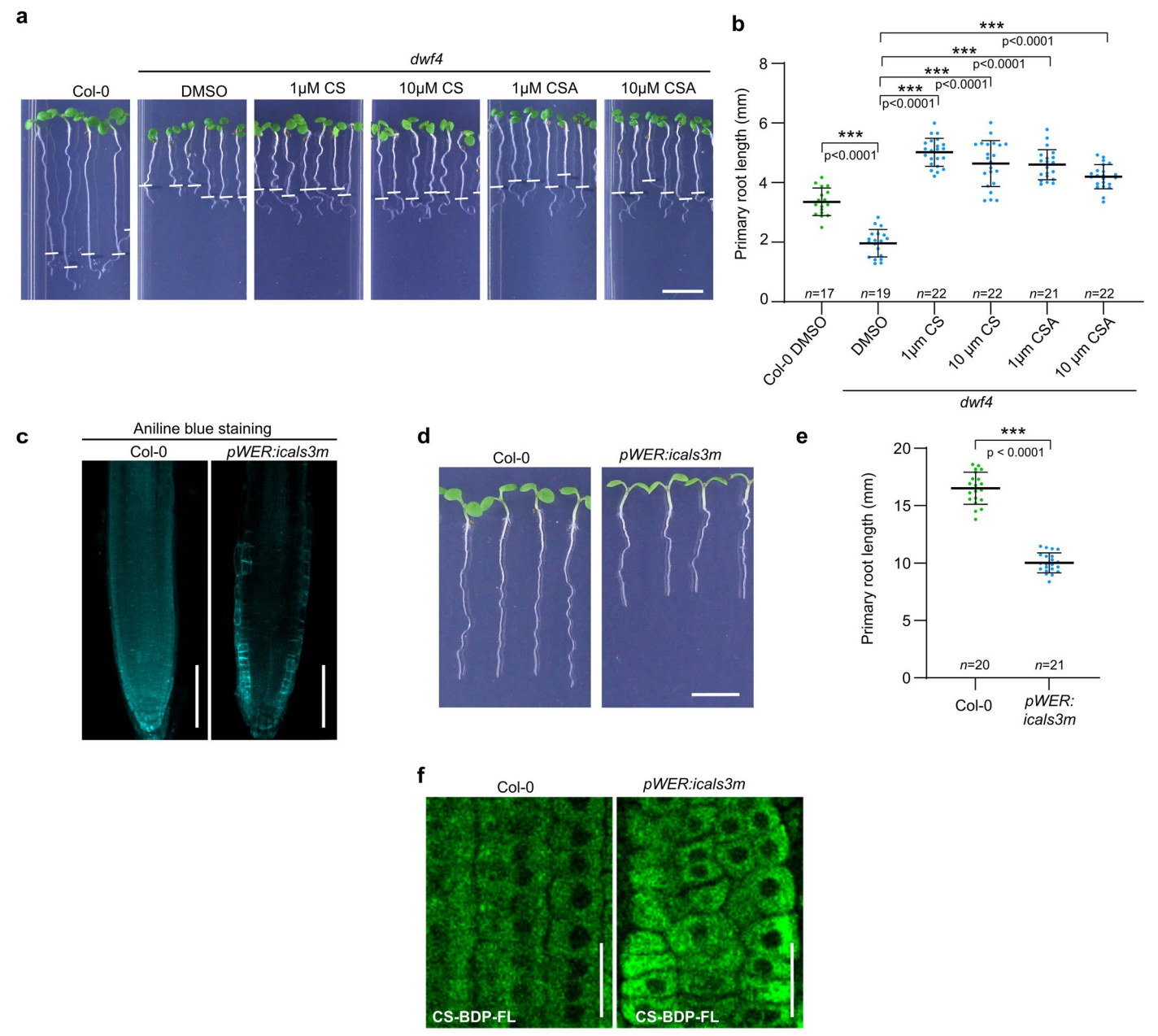
status of BES1 detected by immunoblotting with α -BES1 antibody in whole seedlings. Tubulin detected with α - tubulin antibody was used as loading control. pBES1, phosphorylated BES1, dBES1, dephosphorylated BES1. **h**, Quantification of BES1 dephosphorylation in (**g**) represented as a ratio of dephosphorylated BES1 (dBES1) relative to the total BES1. pBES1, phosphorylated BES1. **i**, The relative gene expression of *DWF4* in Col-0 and PdBG1-OE line. Error bars represent the s.d. For **h,i**, the significant difference was determined with two-tailed Student's unpaired *t*-test analysis. ***P< 0.001, **P< 0.01, and *P< 0.05. For **c,d,e,f**, the experiment was done in two and for **g,h,i**, in three independent biological repeats with similar results.



Extended Data Fig. 4 | See next page for caption.

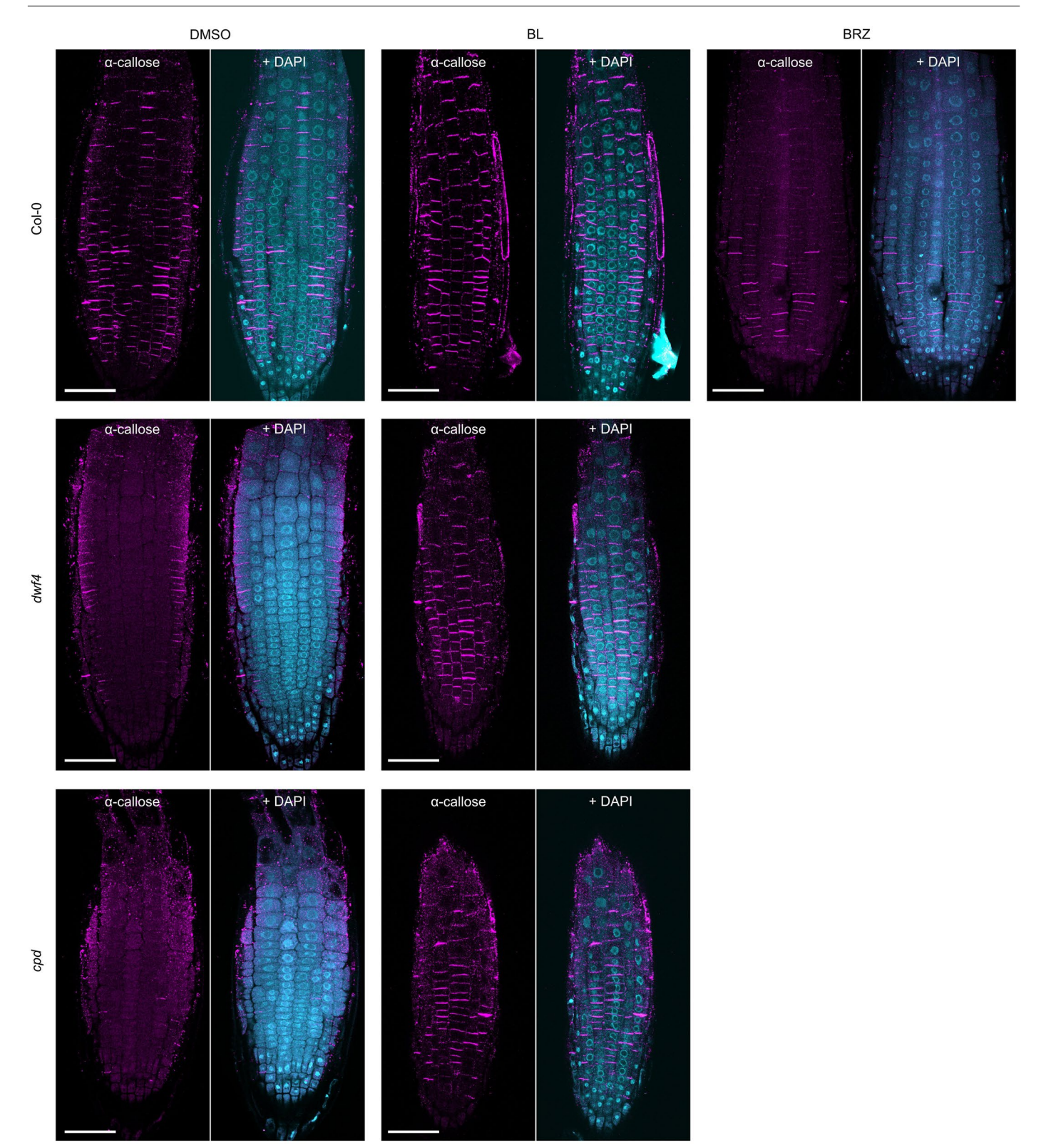
Extended Data Fig. 4 | **22-Hydroxycampesterol (22-OHCR) is an inactive BR precursor. a**, BR biosynthetic pathway with all known enzymes and their presumed position within the pathway. The position of 22-OHCR is highlighted. **b**, 22-OHCR rescued the root phenotype of *dwf4*, but not of *cpd*. Five-day-old *Arabidopsis* wild type (Col-0), *dwf4*, and *cpd* seedlings were transferred to agar medium containing BL (500 pM), 22-OHCR (500 nM), and DMSO (mock), and imaged after 24 h. Root tips were marked immediately after the transfer (white bars). Scale bars, 5 mm. **c**, Quantification of the primary root length of Col-0, *dwf4* and *cpd* in (**b**). Horizontal and error bars represent the means and the s.d., respectively. *n*, number of roots analyzed. The significant differences between the wild type (Col-0) and the mutants were determined with one-way analysis

of variance (ANOVA) and Tukey's multiple comparison tests. *** $P < 0.001 \, \mathbf{d}$, Phosphorylation status of BES1 detected by immunoblotting (IB) with the α -BES1 antibody in seedlings in (\mathbf{b}). Tubulin detected with the α -tubulin antibody was used as loading control. pBES1, phosphorylated BES1, dBES1, dephosphorylated BES1. \mathbf{e} , Confocal images of 6-day-old root tips of pBES1:gBES1-GFP/pEN7:icals3m/dwf4Arabidopsis seedlings stained with PI. Scale bars, 100 μ m. $\mathbf{f}.\mathbf{g}$, Quantification of the meristem cell length (\mathbf{f}) and root meristem diameter (\mathbf{g}) of roots shown in (\mathbf{e}). Horizontal and error bars represent the means and s.d., respectively. n, number cells. The significant differences were determined with one-way analysis of variance (ANOVA) and Tukey's multiple comparison tests. *** P < 0.001. For $\mathbf{b}, \mathbf{c}, \mathbf{d}, \mathbf{e}, \mathbf{f}, \mathbf{g}$, the experiment was repeated twice with similar results.



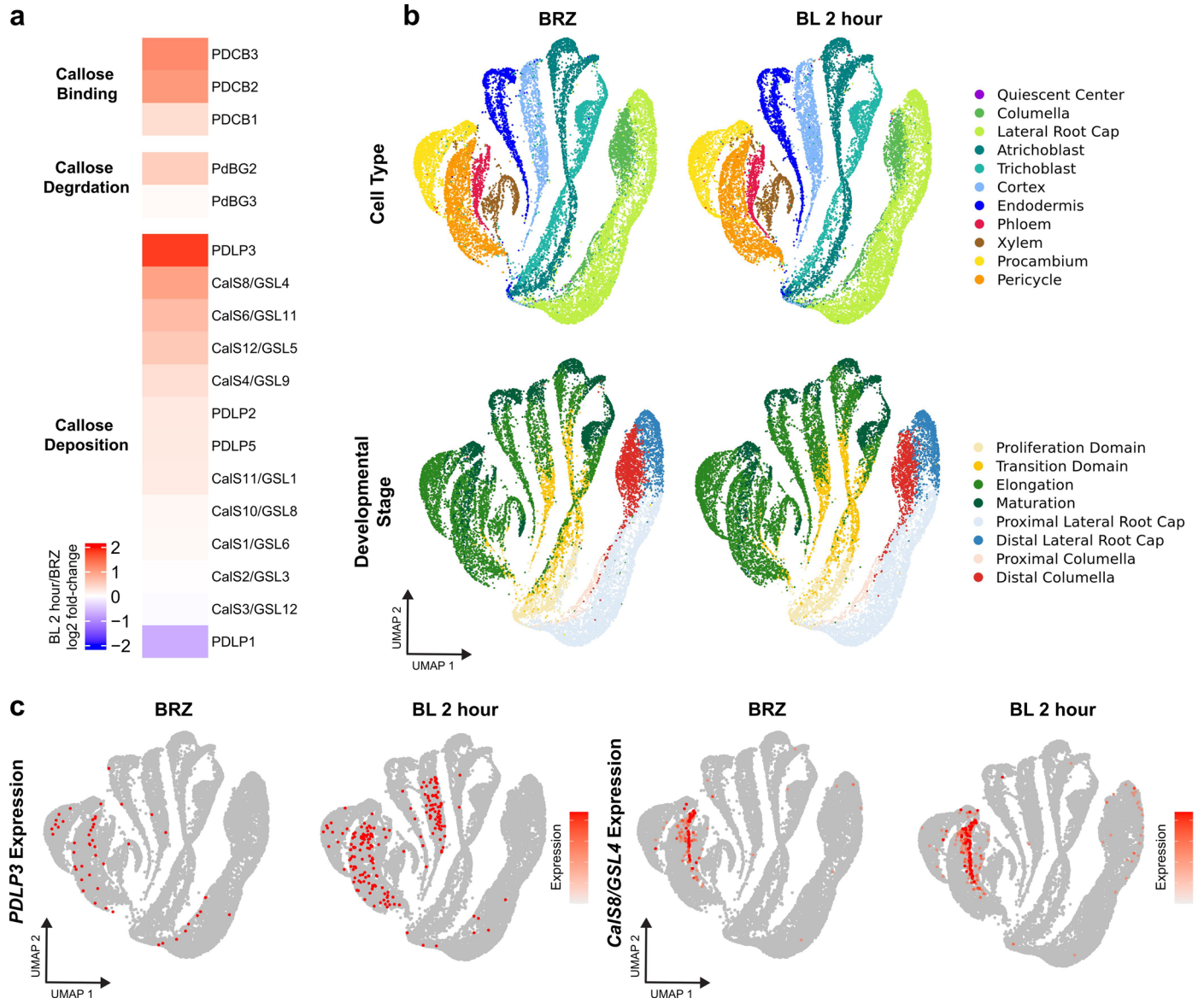
Extended Data Fig. 5 | **Biological activity and uptake of castasterone-alkyne (CSA). a**, CSA retains the biological properties of castasterone (CS). Five-day-old seedlings were transferred to agar media containing different concentrations of CS or CSA as indicated and DMSO (mock) for 24 h. Root tips were marked immediately after the transfer (white bars). Scale bar, 5 mm. **b**, Quantification of primary root length in **(a)**. Horizontal and error bars represent the means and the s.d., respectively. *n*, number of roots analyzed. The significant differences were determined with one-way analysis of variance (ANOVA) and Tukey's multiple comparison tests. *****P* < 0.001 **c**, Aniline blue staining of callose deposition in

6-day-old pWER:icals3m plants. Wild type (Col-0) was used as control (left panel). Scale bars, 100 μ m. **d**, Phenotypes of 6-d-old wild type (Col-0) and pWER:icals3m seedlings. Scale bar, 5 mm. **e**, Quantification of primary root length in (**c**). Horizontal and error bars represent the means and the s.d., respectively. n, number of roots analyzed. The significant differences were determined with two-tailed Student's unpaired t-test analysis. *** P < 0.001. **f**, Accumulation of CS-BDP-FL signal in in the epidermal cells of Col-0 and pWER:icals3m 6-d-old seedlings. Scale bars, 25 μ m. For **a,b,d,e**, the experiment was repeated twice with similar results.



Extended Data Fig. 6 | BRs positively regulate callose deposition in roots. Callose immunostaining of Arabidopsis wide type (Col- 0), dwf4 and cpd roots. Four-day-old seedlings were transferred to agar medium containing brassinolide (BL) (200 nM), brassinazole (BRZ) (1 μ M) and DMSO (mock) for 24 h. Cell nuclei

were stained by 4′,6-diamidino-2-phenylindole (DAPI). Epidermal cell layers are shown. Scale bars, 50 μ m. The same experimental material was used to quantify callose deposition at PD in Fig. 4b.



Extended Data Fig. 7 | Expression levels of callose deposition-related genes are positively regulated by BRs. a, Heatmap showing relative expression of PD-related genes across all cells from publicly available brassinolide (BL) 2-hour scRNA-seq compared to brassinazole (BRZ) scRNA-seq. Color represent log2 fold-change of BL 2-hour versus BRZ. b, Two-dimensional uniform manifold

approximation and projection (UMAP) embedding of BRZ and BL 2-hour treated cells from scRNA-seq dataset 36 . Colors indicate cell type (top) or developmental stage (bottom). \mathbf{c} , PDLP3 and CalS8/CSL4 expression in BRZ and BL 2-hour scRNA-seq. The color scale on the UMAP projection represents log-normalized, corrected UMI counts.

nature research

	Eugenia Russinova
Corresponding author(s):	Nemanja Vukašinovi

Last updated by author(s): Apr 11, 2023

Reporting Summary

Nature Research wishes to improve the reproducibility of the work that we publish. This form provides structure for consistency and transparency in reporting. For further information on Nature Research policies, see our <u>Editorial Policies</u> and the <u>Editorial Policy Checklist</u>.

\sim			
St	at	rist	יורי

FOr	an st	atistical analyses, confirm that the following items are present in the figure legend, table legend, main text, or Methods section.
n/a	Cor	nfirmed
	\boxtimes	The exact sample size (n) for each experimental group/condition, given as a discrete number and unit of measurement
	\boxtimes	A statement on whether measurements were taken from distinct samples or whether the same sample was measured repeatedly
	\boxtimes	The statistical test(s) used AND whether they are one- or two-sided Only common tests should be described solely by name; describe more complex techniques in the Methods section.
X		A description of all covariates tested
X		A description of any assumptions or corrections, such as tests of normality and adjustment for multiple comparisons
	\boxtimes	A full description of the statistical parameters including central tendency (e.g. means) or other basic estimates (e.g. regression coefficient AND variation (e.g. standard deviation) or associated estimates of uncertainty (e.g. confidence intervals)
	\boxtimes	For null hypothesis testing, the test statistic (e.g. <i>F</i> , <i>t</i> , <i>r</i>) with confidence intervals, effect sizes, degrees of freedom and <i>P</i> value noted <i>Give P values as exact values whenever suitable.</i>
\boxtimes		For Bayesian analysis, information on the choice of priors and Markov chain Monte Carlo settings
\boxtimes		For hierarchical and complex designs, identification of the appropriate level for tests and full reporting of outcomes
\boxtimes		Estimates of effect sizes (e.g. Cohen's d, Pearson's r), indicating how they were calculated

Our web collection on <u>statistics for biologists</u> contains articles on many of the points above.

Software and code

Policy information about availability of computer code

Data collection

- Image collection: Las-X software (v 3.5.0.18371) for the Leica SP8 confocal microscope and ZEISS ZEN 3.3 (blue edition) software for Zeiss LSM 880 and Zeiss LSM 900 microscopes.

- Immunoblotting: Image Lab Software 3.0 (Bio-RAD).
- The heatmap was visualized with ComplexHeatmap (v2.10.0); Gu et al., 2016, Bioinformatics.

Data analysis

- For image analysis: Image) and FIJI (https://imagej.nih.gov/ij/).
- $For \ statistical \ data \ analysis: Microsoft \ Excel \ and \ GraphPad \ Prism \ v_8.0 \ \& \ v_9.0 \ (https://www.graphpad.com/).$

For manuscripts utilizing custom algorithms or software that are central to the research but not yet described in published literature, software must be made available to editors and reviewers. We strongly encourage code deposition in a community repository (e.g. GitHub). See the Nature Research guidelines for submitting code & software for further information.

Data

Policy information about availability of data

All manuscripts must include a data availability statement. This statement should provide the following information, where applicable:

- Accession codes, unique identifiers, or web links for publicly available datasets
- A list of figures that have associated raw data
- A description of any restrictions on data availability
- We provided all raw data (e.g. statistical analysis and raw blots with repeats).
- To examine the transcriptional regulation of PD-related genes by BRs, we reanalyzed a previously described scRNA-seq dataset (GEO: GSE212230); Nolan et al., 2023, Science.

Field-spe	cific reporting					
Please select the or	ne below that is the best fit for your research. If you are not sure, read the appropriate sections before making your selection.					
Life sciences	Behavioural & social sciences Ecological, evolutionary & environmental sciences					
For a reference copy of t	he document with all sections, see <u>nature.com/documents/nr-reporting-summary-flat.pdf</u>					
Life sciences study design						
	close on these points even when the disclosure is negative.					
Sample size	No statistical method was used to predetermine sample size. Sample size was determined based on empirical knowledge and previous publications with similar content (Vukasinovic et al., 2021, Nature Plants; Nolan et al., 2023, Science).					
Data exclusions	No data was excluded.					
Replication	All experiments were performed at least 2 or 3 times with similar outcomes.					
Randomization	Samples were not randomized because in most of the experiments plant responses to different conditions were measured (e.g. hormone or hormone precursor). In these cases, plants were positionally randomized in multi-chamber dishes. Plants were randomly collected for further analysis (e.g. microscopy).					
Blinding	Blinding was not applied. In some cases phenotypic differences were obvious to researchers, so they knew at every point what phenotype/ treatment is being observed. Key results (such as CSA click chemistry) were observed independently by at least two members of the team.					
	g for specific materials, systems and methods on from authors about some types of materials, experimental systems and methods used in many studies. Here, indicate whether each material,					
system or method list	ed is relevant to your study. If you are not sure if a list item applies to your research, read the appropriate section before selecting a response.					
Materials & experimental systems Methods						
n/a Involved in th						
Antibodies ChIP-seq						
	Eukaryotic cell lines Flow cytometry					
Palaeontology and archaeology MRI-based neuroimaging						
Animals and other organisms						
Human research participants Clinical data						
Dual use research of concern						
Antibodies						
Antibodies used	Comercial antibodies: - Anti-Tubulin antibody [YOL1/34] (Abcam, ab6161) Dilution 1:5000 Donkey Anti-Rabbit IgG (Merck, NA934V); Dilution 1:10000.					

- Sheep Anti-Mouse IgG (Merck, NA931V). Dilution 1:10000.
- Callose monoclonal antibody (1-3)-beta-glucan-directed monoclonal, (Mouse IgG, KAPPA LIGHT) Biosupplies Australia, Cat. No. 400-2. Dilution 1:500.
- Goat anti-Mouse IgG (H+L) Cross-Adsorbed Secondary Antibody, Alexa Fluor" 594 Invitrogen. Dilution 1:500.
- Rabbit BES1 polyclonal antibody was provided by Yanhai Yin. Dilution 1:5000.

Validation

- $Anti-Tubulin \ antibody \ [YOL1/34]: https://www.abcam.com/tubulin-antibody-yol134-microtubule-marker-ab6161.html$
- $\ BES1 \ polyclonal \ antibody: Yin \ et \ al. \ 2002, \ https://doi.org/10.1016/S0092-8674(02)00721-3$
- Callose monoclonal antibody is widely used (Park et al., 2001; Platre et al., 2022)
- Goat anti-Mouse Alexa Fluor" 594 is a widely used commercial antibody